A Szilikátipari Tudományos Egyesület lapja

építőanyag

Journal of Silicate Based and Composite Materials

A TARTALOMBÓL:

2019/6

TURKEYTRIB 2020 3rd INTERNATIONAL CONFERENCE ON TRIBOLOGY

June 18-20 2020

CONFERENCE VENUE: Elite World Prestige Hotel
ADDRESS: Şehit Muhtar Caddesi No:40, 34435 Taksim Istanbul-TURKEY
WELCOME TO TURKEYTRIB 2020!

We are very pleased to announce that the 3rd International Conference on Tribology TURKEYTRIB 2020 will be held from 18 to 20 June 2020 at the Elite World Prestige Hotel Taksim-İstanbul-TURKEY. The scope of this conference embraces the state of art and future trends in tribology research and application, emphasizing the necessity of facilitation intellectual collaboration across both disciplinary and national-international boundaries. The main objective of the conference is to provide a unique opportunity of presenting and discussing recent developments in different aspects of Tribology and strengthen the linkage between academia and industry. The conference consists of scientific sessions, symposia on specific topics, exhibitions and various collateral events. Turkish and Foreign groups of experts will have chance to share information and get in touch with other groups in all part of Tribology. Nowadays these aspects are becoming more and more important both in respect of human life and environment.

– SPECIAL ISSUE (Web of Science Core Collection-Emerging Sources Citation Index): Selected high-quality papers (10) presented at the TurkeyTrib'20 conference will be selected and invited to submit their contributions for Special Issue publication in Építőanyag - Journal of Silicate Based and Composite Materials. (SCIE; Impact Factor 1.079 (2018). The submission due is 30 June 2020.

www.turkeytribconference.com/index.php/en/

TURKEYTRIB 2020
3rd INTERNATIONAL CONFERENCE TRIBOLOGY
18-20 JUNE
ELITE WORLD PRESTIGE HOTEL-TAKSIM
ISTANBUL-TURKEY

építőanyag

Journal of Silicate Based and Composite Materials

2019/6

TARTALOM

CONTENT

A finomkerámia-, üveg-, cement-, mész-, beton-, tégla- és cserép-, kő- és kavics-, tűzállóanyag-, szigetelőanyag-iparágak szakmai lapja
Scientific journal of ceramics, glass, cement, concrete, clay products, stone and gravel, insulating and fireproof materials and composites

A folyóiratot referálja · The journal is referred by:

A folyóiratban lektorált cikkek jelennek meg.
All published papers are peer-reviewed.
Kiadó · Publisher: Szilikátipari Tudományos Egyesület (SZTE)
Elnök · President: ASZTALOS István
1034 Budapest, Bécsi út 122–124.
Tel.: +36-1/201-9360 ▪ E-mail: epitoanyag@szte.org.hu
Tördelő szerkesztő · Layout editor: NÉMETH Hajnalka
Címlapfotó · Cover photo: GYURKÓ Zoltán

WWW.EPITOANYAG.ORG.HU
EN.EPITOANYAG.ORG.HU

Online ISSN: 2064-4477
Print ISSN: 0013-970x
INDEX: 2 52 50 ▪ 71 (2019) 179–210

Synthesis of hydrogarnets in the system $Al_2O_3 \cdot 2SiO_2$-SiO_2-CaO-H_2O under hydrothermal conditions

Zdzisław PYTEL ▪ AGH University of Science and Technology, Faculty of Materials Science and Ceramics, Poland ▪ pytel@agh.edu.pl

Érkezett: 2019. 11. 29. ▪ Received: 29. 11. 2019. ▪ https://doi.org/10.14382/epitoanyag-jsbcm.2019.31

Zdzisław PYTEL
is a Doctor in Department of Building Materials Technology, Faculty of Materials Science and Ceramics, AGH University of Science and Technology, Cracow, Poland. His special field is utilization of waste by-products (especially fly ashes) in ceramic building materials made from clays and in the range of cementitious materials in concrete technology. He has worked for many years projects connected with sand-lime bricks production.

Abstract

The paper summarises the experimental data on the products of synthesis of mixtures containing metakaolinite (AS_2), silica (SiO_2) and lime (CaO) in various proportions, under hydrothermal conditions at 180°C. The actual compositions of reacting mixtures were determined by the molar ratios Ca/(Al+Si), Al/(Si+Al) and C/S, in the respective ranges (0.75÷1.5), (0.2÷0.5) and (1.0÷3.0). Compositions of the reacting mixtures correspond to stoichiometric ratios of particular oxides, being the components of hydrogarnets from the series C_3AS_3 – C_3AH_6, whose composition varies in accordance with the formula $Ca_3Al_2(SiO_4)_{3-x}(OH)_{4x}$, for x in the range (0.0-2.0). The mineralogical characteristic of thus obtained products of synthesis are evaluated basing on XRD, DTA, TG, IR and SEM+EDAX test data. Results obtained to date reveal that the hydrogarnet C_3AH_6 is the most frequent product obtained in the analysed systems. It coexists with other products of the synthesis, belonging to the group of hydrated calcium silicates, chiefly revealed as an amorphous phase C-S-H and tobermorite ($C_5S_6H_5$).

Keywords: metakaolinite, hydrogarnets, hydrated calcium silicates, hydrothermal conditions
Kulcsszavak: metakaolinit, hidrogénhidrát, hidratált kalcium-szilikátok, hidrotermikus körülmények

1. Introduction

Hydrogarnets of the series $A_3B_2\{[TO_4]_{3-x}(OH)_{4x}\}$, *x* ranging from 1 to 3, have the structure of garnets in which the process of partial or complete isomorphic substitution occurs, referred to as '*hydrogarnet substitution*', in accordance with the formula $4(OH)^- \leftrightarrow (SiO_4)^{4-}$. Cations of metals A and B occur in respective configurations 8 and 6 and the tetrahedron, cation T is mostly silicon [1]. Because of the possibility of isomorphic substitution as a continuous process, a series of solid solutions will be formed, their names depending on extreme terms in the given series [2]. Grossular ($Ca_3Al_2[SiO_4]_3$) - hydrogarnet ($Ca_3Al_2(OH)_{12}$) is a well known hydrogarnet series whose elemental composition varies in accordance with the general formula $Ca_3Al_2\ [SiO_4]_{3-x}(OH)_{4x}$ [3]. It is assumed that those structures in the series are most stable in which *x = 1*, for example hydrogrossular ($Ca_3Al_2[SiO_4]_2(OH)_4$). This series is of great importance in the sector of manufacturing of construction materials based on mineral binders in the form of cement or lime [4-6]. This series is of particular importance for ceramic engineers since its components determine the functional features of those construction materials, particularly their durability and strength, in the context of their susceptibility to carbonisation. These impacts, however, are not clearly defined, as several aspects are involved, yet it is a well-established fact that the higher the silica contents in hydrogarnets, the better the chemical resistance of construction materials containing those mineral binders.

Depending on the extent of '*hydrogarnet substitutions*', physical properties of individual components of the series of solid solutions will vary [7, 8]. In the case of the series C_3AS_3 – C_3AH_6, the increase in the number of substitutions of the tetrahedrons $[SiO_4]^{4-}$ by the complex $[(OH)_4]^{4-}$ is accompanied by the continuous change (increase) of the elementary cell parameters, from a_o = 1.185 for grossular to a_o = 1.256 for hydrogarnete. Furthermore, as the number of complexes $[(OH)_4]^{4-}$ increases, apart from the lattice parameters, the position and intensity of reflexes will change, too. Besides, some diffraction lines will disappear whilst new ones will appear instead. At the same time, the growth of the elementary cell is accompanied by the decrease of the refractive index 'n' from 1.743 for C_3AS_3 to 1.605 for C_3AH_6 and by the change of density. With the increase of the amount of water present in the hydrogarnete structure in the form of hydroxyl groups, the dehydroxylation effect becomes more intense and the temperature of its maximum on the DTA curve goes down from about 750-850°C for C_3AS_3 to (350-500)°C for C_3AH_6 [9-11].

2. Materials

Reaction mixtures for the synthesis of hydrogarnets contain the following materials:

- metakaolinite METASTAR 501 (symbol ME) whose composition is shown in *Table 1*.
- burnt lime obtained by calcination analytically pure $CaCO_3$ at the temperature 1050°C for 3 hours (symbol C)
- silica powder (manufacturer: Quartzwerke GmbH), commercially available as SIKRON-Feinstmehl SGL-300 (symbol S)
- analytically pure aluminium oxide γ-Al_2O_3 (symbol A)
- distilled water (symbol H)

SiO_2	Al_2O_3	CaO	MgO	Fe_2O_3	Na_2O	K_2O	TiO_2	MnO	P_2O_5	L.I.O
52.22	41.41	0.08	0.26	0.49	0.01	1.73	0.01	0.01	0.13	1.66

Table 1 Chemical analysis of metakaolinite METASTAR 501
1. táblázat METASTAR 501 metakaolinit kémiai elemzése

3. Experimental

The synthesis of hydrogarnets of the series C_3AS_3 – C_3AH_6 was conducted under hydrothermal conditions. Chemical composition of the reaction mixtures was varied, determined by the relevant molar ratios: C/(S+A), A/(S+A) and C/S. Those molar rations were determined by the complex value *x* present in the general formula defining the composition hydrogarnets of the given series. For each considered value of *x* a reaction mixture was prepared in the form of dry components, whose chemical composition would represent the theoretical hydrogarnate composition for the given value of *x*. Synthesis of hydrogarnets was conducted for the following values of *x*: 0; 1.0; 1.5; 2.0. Accordingly, the formulas expressing the composition of particular hydrogarnets and the corresponding molar ratios agree well with the data in *Table 2.*

Sample designation	Value of „x"	Hydrogarnet formula	Molar ratios		
			C/S	C/(S+A)	A/(S+A)
ME – 0	0	$C_3Al_2[SiO_4]_3$ ($3CaO{\cdot}Al_2O_3{\cdot}3SiO_2$, C_3AS_3)	1.0	0.75 (3/4)	0.25 (1/4)
ME – 1	1.0	$C_3Al_2[SiO_4]_2(OH)_4$ ($3CaO{\cdot}Al_2O_3{\cdot}2SiO_2{\cdot}2H_2O$, $C_3AS_2H_2$)	1.5	1.0	0.33 (1/3)
ME – 1.5	1.5	$C_3Al_2[SiO_4]_{1.5}(OH)_6$ ($3CaO{\cdot}Al_2O_3{\cdot}1.5SiO_2{\cdot}3H_2O$, $C_3AS_{1.5}H_3$)	2.0	1.2 (6/5)	0.4 (2/5)
ME – 2	2.0	$C_3Al_2[SiO_4](OH)_8$ ($3CaO{\cdot}Al_2O_3{\cdot}SiO_2{\cdot}4H_2O$, C_3ASH_4)	3.0	1.5	0.5

Table 2 Chemical composition of synthesised hydrogarnets
2. táblázat A szintetizált hidrogarnetek kémiai összetétele

Reaction mixtures are prepared in stabilised and reproducible conditions. The procedure involved weighing the required amounts of basic components: metakaolinite (ME) and lime (C). Furthermore, certain amounts of silica powder (S) or aluminium oxide (A) were added to make up for the deficiency of silica or aluminium in metakaolinite and to obtain the desired chemical composition of reaction mixtures, determined by the molar ratios given in *Table 2.* Afterwards the mixtures are homogenised in an agate mortar, in the first stage with no presence of water, and then with water added. The amount of distilled water added to the mixture is determined by the need to ensure the complete hydration of calcium oxide and to achieve such consistency of the slurry that the ratio of water 'w' to dry substances 's' should equal 0.8. Thus prepared slurry is then transferred to Teflon crucibles which are then placed inside pressure cylinders acting as laboratory autoclaves. The slurry is then subjected to hydrothermal treatment. The samples are autoclaved at the temperature 180°C, which corresponds to the saturated vapour pressure of 1.002 MPa, for a variable period of time: 8, 24 and 72 hours. The time required to reach the specified conditions is about 1.5 hours and the autoclaves are cooled down to the ambient temperature in an unconstrained manner.

The phase composition of thus obtained materials is analysed using the XRD, DTA, TG, IR and SEM+EDAX methods.

4. Results

The analysis of the phase composition of thus obtained products uses mostly the XRD data. X-ray tests were performed using an X-ray diffractometer (Philips PW 1040). X-ray patterns were registered in the angle range CuK_α 5 - 60° 2θ and the presence of mineral phases was established on the basis of ICPDS-ICDD file Copyright 2005. Test results in the form of XRD data are compiled in *Fig. 1.*

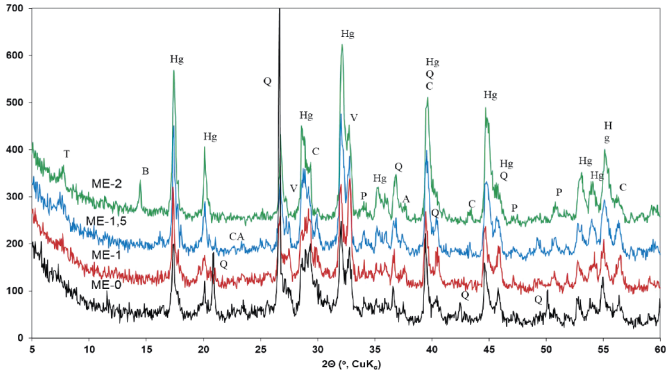

Fig. 1 XRD data of samples synthesised for 24 hours
1. ábra A 24 órán át szintetizált minták XRD adatai

Designations: Hg-hydrogarnate; Q-quartz; P-portlandite; C- calcite; V-vaterite; B-boehmite; A- aluminium oxide; CA-carboaluminate; T- tobermorite;

IR spectra (400 – 4000 cm^{-1}) are registered using the standard technique involving the KBr tablet transmission. Measurements are taken with a Fourrier spectometer Bio-Rad FTS 60MV with the resolution capacity 4 cm^{-1} for 256 repetitions. Test results in the form of IR spectra of the investigated samples are shown in *Fig. 2.*

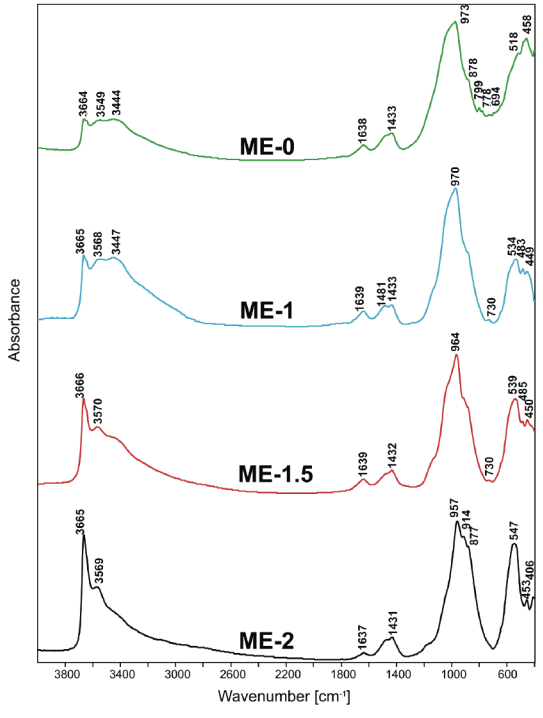

Fig. 2 IR spectra of the investigated materials
2. ábra A vizsgált anyagok IR-spektrumai

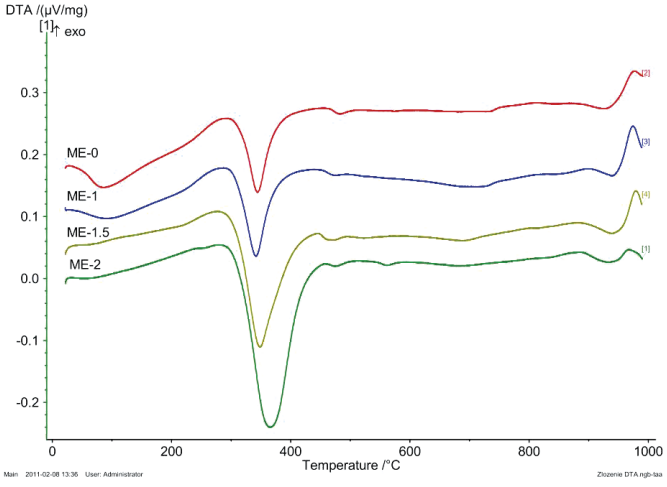

a)

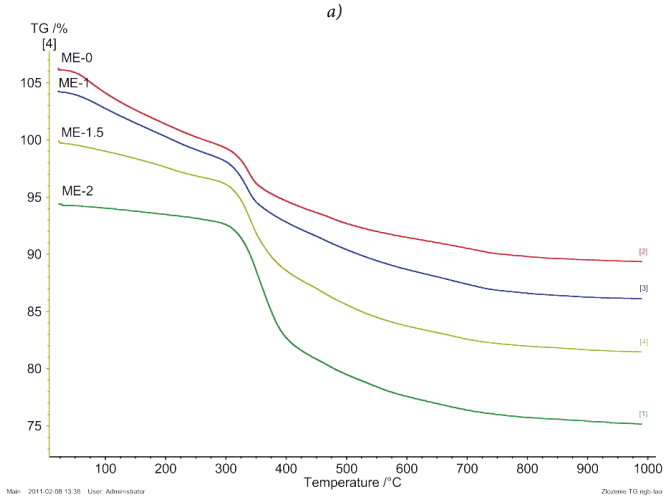

b)

Fig. 3 Thermal treatment data: a) DTA curves; b) TG curves
3. ábra Hőkezelési adatok: a) DTA görbék; b) TG görbék

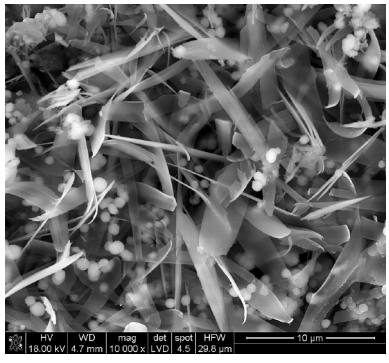

a) ME-0

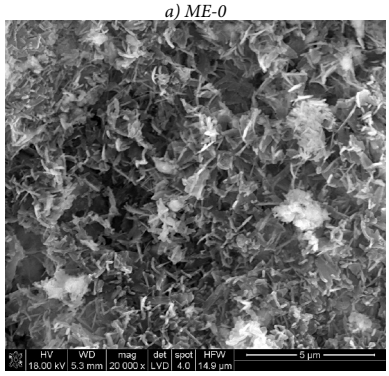

b) ME-1

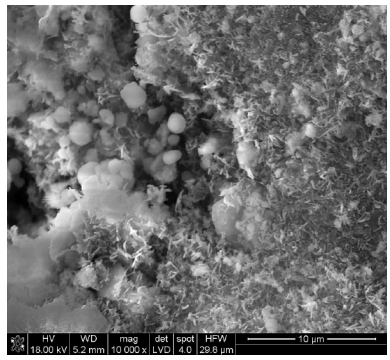

c) ME-1.5

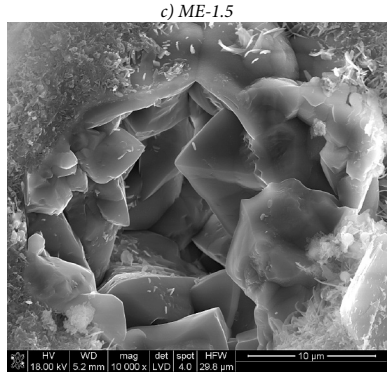

d) ME-2

Fig. 4 Microstructure of investigated materials
4. ábra A vizsgált anyagok mikroszerkezete

Investigations by the thermal methods DTA and TG are conducted using the device NETZSCH STA 449 F30 *Jupiter*. Measuring is done on the carrier DTA-TG, in the temperature range 20-1000°C, the heating rate 10°C/min, in the presence of air with Al_2O_3 in the crucibles. Test results in the form of DTA and TG curves are shown in *Fig. 3*.

The microstructure of autoclaved materials is analysed using a scanning microscope $NOVA_{NANO}$ SEM 200 (FEI COMPANY) equipped with a micro-analyser EDAX. Samples to be tested are first sprinkled with coal powder. The most distinctive images of microstructure of investigated sample profiles are shown in *Fig. 4*.

5. Discussion

The analysis of X-ray test data (*Fig. 1*) reveals that for each investigated sample the basic product of synthesis will be hydrogarnete, accompanied by tobermorite. Furthermore, for hydrogarnets we observe most characteristic line shifting for the specified value of 'd', which evidences the formation of solid solutions. The locations of reflexes from the planes (2,1,1) and (6,4,0) and their half-width indicate that in each case we obtain a hydrogarnete, whose composition varies in accordance with the Vegard's law (correlation factor 0.999), for *x* ranging from 2.38 to 2.65. It is reasonable to suppose that the composition of this product falls between the compositions of hydrogarnets given by the formulas: $C_3Al_2(SiO_4)_{0.62}(OH)_{9.5}$ and $C_3Al_2(SiO_4)_{0.35}(OH)_{10.6}$. Actually, that means that in each case the recorded extent of silica substitutions ('*hydrogarnet substitution*') is less than the predicted (theoretical) value [8, 12].

The analysis of IR spectra in *Fig. 2* reveals that the band responsible for OH^- group substitutions is that registered for the wave number 3666 cm^{-1}. Its intensity grows with the increasing number of substitutions, and its small half-width is indicative of the fact that OH^- groups are distributed in an ordered manner within the structure of the material. The spectral line 3570 cm^{-1} displays similar though less pronounced behaviour. The spectral line corresponding to the wave number 3400 cm-1 displays an entirely different behaviour and the large band half-width indicates that it can be associated with tensile vibrations of OH^- groups, distributed in the statistical manner in the structure of the material, or, more probably, it can be associated with water molecules physically connected with the material's surface. This conclusion can be drawn from the changes of the band intensity correlated with that of the spectral line 1630 cm^{-1}, associated with deformative vibrations of H-O-H within the water molecule [13].

The IR spectrum for the sample ME - 0 reveals a spectral line 973 cm^{-1}, indicative of the occurrence of asymmetric tensile vibrations in Si-O and the spectral line 458 cm^{-1} associated with bending vibration in SiO_4 tetrahedrons, which is a distinctive feature of ortho-silicates, including hydrogarnets. The spectrum also reveals the presence of a doublet of spectral lines 780-800 cm^{-1}, indicative of vibrations symmetrically stretching the Si-O-Si bridges, which is a distinctive feature of β-quartz. This doublet is absent in subsequent spectra, which suggests that the samples do not contain free quartz. Furthermore, a spectral line is revealed corresponding to the wave number 914 cm^{-1}, characteristic of Al-OH vibrations (LK_{Al} = 6, octahedron). The band intensity tends to increase in subsequent spectra, which can indicate that a part of OH^- groups are associated with aluminium, specifically with AlO_4 tetrahedrons. Of particular importance is the fact that position of a band with the highest intensity tends to shift from the wave number 973 cm^{-1} (sample ME - 0) to 957 cm^{-1} (sample ME - 2), which can indicate that substitutions of OH^- groups in a large extent depolymerize the structure, which tends towards the ideally mono-silicate structure. Furthermore, the spectra reveal the lines for the wave number 1432 cm^{-1}, associated with CO_3^{2-} groups, which is confirmed by the presence of carbonates.

DTA and TG curves for the investigated materials, shown in *Fig. 3*, are very similar. That can indicate that the analysed samples have a similar composition in qualitative terms. Quantitative differences involve the intensity and temperature of the predominant endothermic peak associated with dehydroxylation of hydragarnets. The enhanced peak intensity and the increase of its maximum temperature from 344.4°C (sample ME - 0, x = 0) to 366.4°C (sample ME - 2, x = 2) evidence the formation of the series of hydrogarnets with the decreasing number of silicate substitutions. However, the scale of the temperature increase suggests that the number of '*hydrogarnate substitutions*' $4(OH)^- \leftrightarrow [SiO_4]^{4-}$ seems inadequate in relation to the specified value of *x*, determining the composition of reaction mixtures. That is why the chemical composition of thus formed hydrogarnets does not represent their predicted (theoretical) composition [14].

The microstructural analysis of investigated samples (*Fig. 4*) reveals the co-existence of two basic products synthesised under hydrothermal conditions: tobermorite formed in the shape of elongated crystals, and hydrogarnets with a typical crystal morphology. In a majority of investigated samples these products form a heterogeneous mixture of statistically distributed crystals.

One can conclude, therefore, that regardless of the initial composition of reaction mixtures, in each case the synthesis conducted under hydrothermal conditions will yield two products with crystalline structure: tobermorite and hydrogarnate, containing silicon. However, the extent of silicate substitutions in the structure of hydrogarnets is lower than expected and fails to reflect the chemical composition of mixtures used in the process of synthesis, no matter what the time of duration.

Acknowledgement

This study is a part of a research project sponsored by the Polish Ministry of Science and Education from the resources allocated for years 2011-2013, as a project No N506 282140.

References

[1] Handke M. (2008): Krystalochemia krzemianów, wyd. II poprawione, Uczelniane Wydawnictwa Naukowo-Dydaktyczne, Kraków (In Polish).

[2] Galuskina, J., Galuskin, E. (2003): Garnets of the Hydrogrossular-Hydroandradite-Hydroschorlomite series, Mineralogical Society of Poland (special papers), Vol. 22, pp. 54 -57.

[3] Nohes, R.H., Akhmatskaya, E.V., Milman, V., White, J.A., Winkler, B., Pickard, C.J. (2000): An ab initio study of hydrogarnets", American Mineralogist, Vol. 85, pp. 1706-1715.

[4] Edited by Peter, C. (1998): Lea's Chemistry of Cement and Concrete, Hewlett Arnold.

[5] Taylor, H.F.W. (1990): Cement Chemistry, Academic Press.

[6] Kurdowski, W. (2010): Chemia Cementu i Betonu. Wydawnictwo Naukowe PWN, Warszawa (In Polish).

[7] Żabiński, W. (1966): Hydrogarnets. Polska Akademia Nauk Oddział w Krakowie, Komisja Nauk Mineralogicznych, Prace mineralogiczne nr 3, Wyd. Geologiczne, Warszawa (In Polish).

[8] Carlom, A.R., Williams, C.D., Fullen, M.A. (2009): Hydrothermal synthesis of hydrogarnet and tobermorite at 195°C from kaolinite and metakolinite in the $CaO-Al_2O_3-SiO_2-H_2O$ system: A comperative study, Applied Clay Science, Vol. 42, pp. 228-237. https://doi.org/10.1016/j.clay.2008.09.014

[9] Klimesh, D.S., Ray, A. (1999): DTA-TG study of the $CaO-SiO_2-H_2O$ and $CaO-Al_2O_3-SiO_2-H_2O$ systems under hydrothermal conditions. Journal of Thermal Analysis and Calorimetry, Vol. 56, pp. 27-34.

[10] Klimesh, D.S., Ray, A. (1998): DTA-TG of unstirred autoclaved metakaolin-lime-quartz slurries. The formation of hydrogarnets. Thermochimica Acta, No. 316, pp. 149-154.

[11] Klimesh, D.S., Ray, A. (1999): DTA-TG evaluations of the $CaO-Al_2O_3-SiO_2-H_2O$ system treated hydrothermally. Termochimica Acta, No. 334, pp. 115-122.

[12] Klimesh, D.S., Ray, A. (1998): Hydrogarnet formation during autoclaving at 180°C in unstirred Metakaolin-Lime-Quartz slurries. CCR, Vol. 28, No. 8, pp. 1109-1117.

[13] Rossman, G.R., Aines, R.D. (1991): The hydrous components in garnets: grossular-hydrogrossular. *Amer. Mineral.*, Vol. 76, pp. 1153–1164.

[14] Jappy, T.G., Glasser, F.P. (1991/92): Synthesis and stability of silica-substituted hydrogarnet $Ca_3Al_2Si_{3-x}O_{12-4x}(OH)_{4x}$. Adv. Cem. Res., Vol. 4, No. 1, pp. 1 - 8.

Ref.:
Pytel, Zdzisław: *Synthesis of hydrogarnets in the system $Al_2O_3 \cdot 2SiO_2$-SiO_2-CaO-H_2O under hydrothermal conditions*
Építőanyag – Journal of Silicate Based and Composite Materials, Vol. 71, No. 6 (2019), 180–183. p.
https://doi.org/10.14382/epitoanyag-jsbcm.2019.31

Rheological behaviour modelling of cement paste with nanotubes and plasticizer

Gintautas SKRIPKIUNAS ▪ Faculty of Civil Engineering, Vilnius Gediminas Technical University, Lithuania ▪ gintautas.skripkiunas@vgtu.lt

Ekaterina KARPOVA ▪ Faculty of Civil Engineering, Vilnius Gediminas Technical University, Lithuania ▪ ekaterina.karpova@vgtu.lt

Mindaugas DAUKSYS ▪ Faculty of Civil Engineering and Architecture, Kaunas University of Technology, Lithuania ▪ mindaugas.dauksys@ktu.lt

Érkezett: 2019. 11. 29. ▪ Received: 29. 11. 2019. ▪ https://doi.org/10.14382/epitoanyag-jsbcm.2019.32

Gintautas SKRIPKIUNAS
Is associate professor in the Vilnius Gediminas Technical University, Department of Building Materials and Fire Safety at VGTU, in Lithuania.

Ekaterina KARPOVA
Is graduated in the Izhevsk State Technical University (ISTU). At present she is a PhD student in the Vilnius Gediminas Technical University, at Department of Building Materials and Fire Safety, in Lithuania.

Mindaugas DAUKSYS
Is professor in the Kaunas University of Technology and senior specialist in the Building Materials and Structures Research Centre, in Lithuania.

Abstract

Rheological properties of cement pastes determine the technological properties of concrete mixtures and have a significant influence on the concrete placement, including pumping, self-compacting, 3D printing and others. The different types of additives and admixtures allow managing by the technological and rheological properties of cement systems. The lignosulphonate (LS), sulfonated naphthalene and melamine formaldehyde (NF), polycarboxylate ether (PCE) and acrylic polymer plasticizers, which change the consistency of concrete mixtures, are more widely used like plasticizing admixtures in construction practice nowadays. The carbon nanotubes are a perspective tool in managing by the rheological and technological properties of concrete in view of their outstanding mechanical, thermal, optical, electrical and some other properties.

The rheological behaviour of cement pastes with nanotubes and different types of polymer plasticizing admixtures was analyzed in the course of the current research using rotating rheometer with coaxial cylinders.

The cement pastes and concrete mixtures have the non-linear shear rate and shear stress dependence and require the application of non-linear rheological models such as Herschel-Bulkley or modified Bingham model. The approximation of experimental flow curves and evaluation of the rheological parameters such as yield stress, plastic viscosity and pseudoplastic indexes were performed based on the Herschel-Bulkley model in the course of the present research.

The testing of cement pastes in the presence of different plasticizing admixtures with and without MWCNT revealed the differences in rheological parameters depended on applied plasticizer. The molecular structure of plasticizing admixtures, small size, high aspect ratio and surface area of MWCNT, physical and chemical interactions between plasticizers and MWCNT can be a reason of observed changes in the rheological properties of cement pastes. The addition of MWCNT contributes to the obtaining of the cement paste of low dilatancy with definite flowability, yield stress and viscosity.

Keywords: cement paste, plasticizer, nanotubes, yield stress, viscosity, rheological model
Kulcsszavak: cementpép, folyósítószer, nanocsövek, folyáshatár, viszkozitás, reológiai modell

1. Introduction

The exploitation properties and durability of concrete structures depend on the properties of concrete mixtures and concrete placement technologies. Pumping of concrete mixtures is one the general way which is used for concrete transportation at the construction sites nowadays. The main rheological properties of concrete mixtures such as yield stress and plastic viscosity can be used for more accurate prediction of concrete mixtures behaviour in the course of a concreting. However, the evaluation of rheological parameters at the construction site is a challenging task caused by the complexity of rheological testing equipment. Therefore, the researchers are searching for a correlation between the main rheological parameters and technological properties of concrete mixtures [1-6]. For example, E. Secrieru et.al. investigated the effect of pumping on the rheological properties of fresh concrete. They performed a full-scale pumping experiment on a ready-mix concrete with the usage of viscometers for rheological test and revealed that pumping increases yield stress and reduces the viscosity of concrete mixture [1]. The research [2] reported the dependence between rheological parameters of concrete mixture and high pressure caused by concrete pumping.

In addition to pumping, the interest of researchers is devoted to the design of self-compacting concrete (SCC) [7-9] and development of 3D concrete printing technologies [10-12]. Based on the rheological parameters, the authors of the research [7] characterized the surface quality of SCC. They established that yield stress lower than 100 Pa and plastic viscosity lower than 10 Pa·s contribute to the surface defects of concrete caused by segregation. As for 3D printing technology, S.C. Paul et.al. studied 3D concrete printing technology and noticed that better pumpability of 3D printable cementitious materials is reached than thixotropy value is greater than 10000 N mm rpm [10].

The fundamental rheological model, which is used for the description of the flow behaviour of cementitious systems, is the Bingham model. The significant amount of researches

demonstrate the usage of this model for the explanation of the rheological behaviour of cement systems [13-15]. The Bingham model characterizes the linear dependence between shear stress (τ) and shear rate (γ) of cement system and is described by the Equation (1):

$$\tau = \tau_0 + \mu_{pl} \cdot \gamma \quad (1)$$

where: τ - shear stress, Pa;
τ_0 - yield stress of the cement paste, Pa;
$\mu_{pl.}$ - plastic viscosity of the cement paste, Pa·s;
γ - shear rate, s^{-1}.

The rheological behaviour of modern concrete modified by different types of additives and admixtures require an application of the non-linear rheological model. The number of research presents the non-linear character of flow behaviour for modified cement systems [16-23]. The Herschel-Bulkley model and modified Bingham model are used to characterize a non-linear flow behaviour of cement systems. They described by the Equations (2) and (3), respectively:

$$\tau = \tau_0 + K \cdot \gamma^n \quad (2)$$

$$\tau = \tau_0 + \mu \cdot \gamma + c \cdot \gamma^2 \quad (3)$$

where: τ - shear stress, Pa;
τ_0 - yield stress of the cement paste, Pa;
K - consistency factor, $Pa \cdot s^n$;
μ - plastic viscosity, Pa·s;
γ - shear rate, s^{-1};
n - shear thinning/ thickening index (n<1; n>1, respectively);
c - second order term, $Pa \cdot s^2$ [16].

The usage of non-linear rheological model, such as Herschel-Bulkley rheological mode enable to derivate the pseudoplastic index of cement systems what is impossible in case of approximation according to the linear Bingham model. For example, A. Yahia tested the rheological behaviour of cement mortar with water-reducing admixtures and established the shear-thickening response of polycarboxylate plasticizer based on the Herschel-Bulkley model [21].

The increasing interest in the improvement of cement composites by addition of nano additives require an understanding of their action mechanism in the cement system. The analysis of rheological properties and their characterization by the rheological models is one of a way to describe the behaviour of nano additives in cement systems. As well as for the usage of chemical and mineral additives in cement paste, the rheological behaviour of nanomodified cement systems is described by non-linear rheological models. The research [23] presents the results of rheological testing of cement pastes modified by nano-SiO_2, nano-TiO_2, carbon nanotubes and nanofibers. The approximation of obtained rheological data was performed by a modified Bingham model.

The present research is focused on the analysis of the influence of different types of plasticizing admixtures (PL) and multi-walled carbon nanotubes (MWCNT) on the rheological behaviour of cement pastes. The rheological parameters were evaluated based on the Herschel-Bulkley model.

2. Materials and testing methods

2.1 Materials

The Portland cement without mineral additives CEM I 42.5 R conforming to EN 197-1 with water consumption of 26.6% and fineness by Blain of 3552 cm^2/g was used as a binder.

The MWCNT suspension was prepared from the pellets "Graphistrength CW 2-45" produced by the company "Arkema" (France). The pellet contains 45wt. % of MWCNT and 55 wt. % of carboxyl methyl cellulose (CMC). The MWCNT was characterized by the filament length of 0.1 –10 μm and the diameter of 15–20 nm. Distilled water was used as a dispersion medium for MWCNT. The lignosulphonate (LS), sulphonated naphthalene formaldehyde (NF) and polycarboxylate ether (PCE) plasticizers were applied in the research as a dispersant to distribute the MWCNT in the volume of water suspension and as a dispersing agent for cement pastes.

2.2 Testing methods

The ultrasonication by using a Bandelin Sonopuls HD 3400 ultrasonic homogenizer (400 W, 20 kHz) with probe VS 200 T (Ø25 mm, amplitude −82 μm) for 6 min was applied to distribute the MWCNT in water. The more detailed description of a homogenization process of MWCNT suspension is presented in the research [14]. 4 types of MWCNT suspensions, including MWCNT suspension without PL and with LS, NF and PCE plasticizers, were obtained. The concentration of PL was of 3.8% in all aqueous MWCNT suspensions excluding MWCNT suspension without PL. The dosage of PL was chosen to reach the dosage of 1% bwoc in cement pastes as more widely used plasticizer dosage in cement systems.

The rheological test was carried out by rotational rheometer Rheotest RN 4.1 with coaxial cylinders (the scheme of cylinder measuring system is presented in *Fig. 1*) according to the mode presented in *Fig. 2* at 5, 60, 120 min after cement paste mixing. 200 g of cement was used for preparing of cement paste for each rheological test. Water to cement ratio (W/C) was 0.30 and 0.25 for cement paste modified by MWCNT suspension without and with PL, respectively. The MWCNT suspensions were used as mixing water for the cement paste modification in the course of the rheological test. MWCNT dosage was of 0.06% bwoc in the course of rheological tests.

The main rheological parameters, such as yield stress (τ_0) and plastic viscosity (μ) were determined in the course of approximation of flow curve (dependence between shear stress (τ) and shear rate (γ) in the range from 0.1 to 100 s^{-1} based on Herschel-Bulkley model.

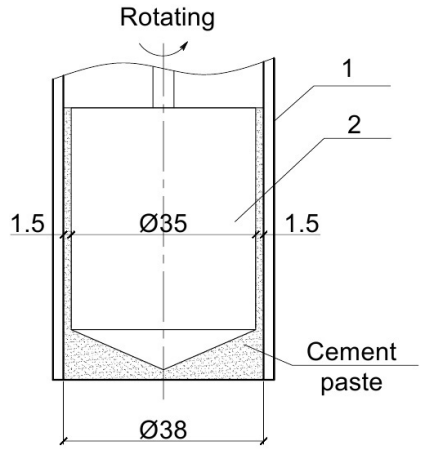

Fig. 1 Scheme of cylinder measuring system Rheotest RN 4.1
1. ábra A Rheotest RN 4.1. mérő rendszer vázlata

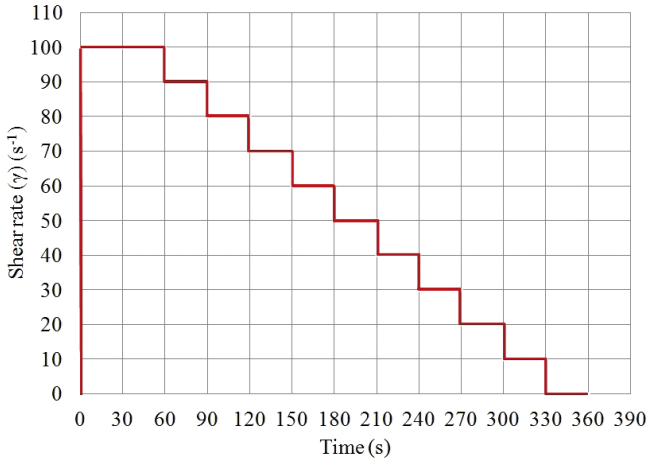

Fig. 2 Shear rate mode of the rheological test
2. ábra A reológiai teszt a nyírási sebesség meghatározásához

3. Results of Investigation

3.1 Influence of chemical admixtures on the flow behaviour of cement paste

The modification of cement paste by PL of different chemical structure leads to the changes in their rheological parameters in different ways. *Fig. 3* represents the flow behaviour of cement pastes without and with the addition of LS, NF and PCE plasticizers in 5 min after cement paste mixing. The approximation of the obtained rheological curves was performed according to the Herschel-Bulkley model. The established rheological parameters, such as plastic viscosity, yield stress and shear thinning/thickening indexes identified the dependence between flow behaviour of cement pastes and applied type of PL. The rheological parameters obtained in the course of the approximation of flow curves by Herschel-Bulkley are listed in *Table 1*.

The significant decrease of yield stress value up to 0.3 Pa was reached in case of application of PCE plasticizer in the cement paste. The yield stress for LS and NF plasticizers were 11.4 and 5.2 Pa, respectively.

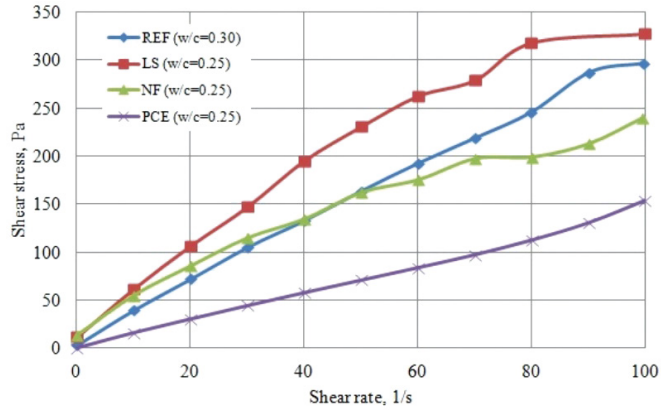

Fig. 3 Flow curves of cement pastes with different PL in 5 min after cement paste mixing
3. ábra Különböző PL tartalmú cementpépek folyási görbéi 5 perc alatt a cementpép keverése után

Specimen	W/C ratio	τ_0, Pa	μ, Pa·s	n
Reference	0.30	3.6	4.0	0.9
LS	0.25	11.4	13.5	0.7
NF	0.25	5.2	6.0	0.8
PCE	0.25	0.3	0.6	1.2

Table 1 Rheological parameters of cement paste with different plasticizing admixtures obtained based on the Herschel-Bulkley model
1. táblázat A Herschel-Bulkley modell alapján kapott különböző folyósítószert tartalmazó cementpépek reológiai paraméterei

The plastic viscosity gained a smaller value for PCE plasticizer and was of 0.6 Pa·s in comparison with plastic viscosity of 13.5 and 6.0 Pa·s for LS and NF plasticizers, respectively.

Also, the difference in the rheological behaviour of the cement pastes with different PL was observed based on pseudoplastic indexes. The LS and NF plasticizers characterized by the indexes 0.7 and 0.8, respectively, that identify their shear-thinning flow behaviour. The cement paste with PCE plasticizer demonstrated the shear thickening flow behaviour with the index of 1.2.

The w/c ratio for the reference sample was of 0.30 caused by testing procedure. The values of the yield stress, plastic viscosity and pseudoplastic index were reached of 3.6 Pa, 4.0 Pa·s and 0.9, respectively. Despite the differences in w/c ratio for the reference sample and samples with PL, it can be concluded that PCE plasticizer has greater plasticizing efficiency in cement paste in comparison with other PL. Mainly, the observed phenomenon can be explained by the differences in the molecular structure of polymers which causes the differences in their action mechanism in the cement systems.

3.2 Influence of MWCNT with and without chemical admixtures on the flow behaviour of cement paste

The present section shows the effect of MWCNT on the rheological behaviour of cement pastes. The separate and combine usage of MWCNT with PL were tested. The flow curves of cement pastes modified by MWCNT with and without PL are presented in *Fig. 4-7*. The values of yield stress, plastic viscosity and shear thinning/ thickening indexes are shown in

Table 2. The values were obtained based on their approximation according to the Herschel-Bulkley rheological model.

Fig. 4 presents the flow curves for cement paste without and with MWCNT prepared in the same w/c ratio of 0.30. The addition of MWCNT to the cement paste leads to the slight increase of yield stress and plastic viscosity in comparison with the reference sample by 8 and 5 %, respectively. The shear thinning index was changed from 0.94 for reference to 0.98 for nanomodified cement paste.

The addition of various types of PL in combination with MWCNT had a different impact on the rheology of cement pastes.

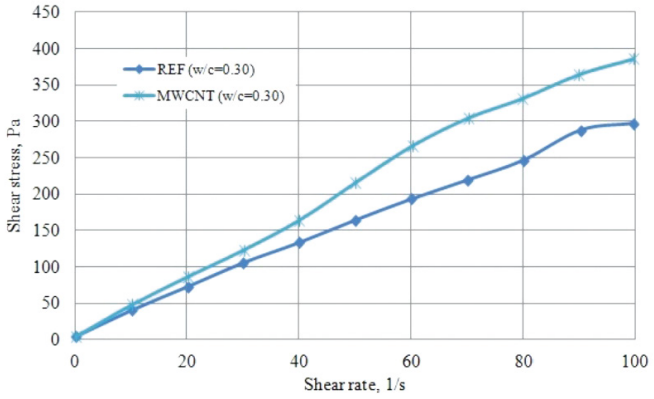

Fig. 4 Flow curves of cement paste with and without MWCNT in 5 min after cement paste mixing
4. ábra A cementpép folyási görbéi MWCNT-vel és anélkül 5 perc alatt a cementpép keverése után

Fig. 5 presents the results of rheological testing of cement pastes modified by MWCNT in the presence of LS plasticizer. The addition of MWCNT to cement paste with LS slightly increases the yield stress by 5% and not significantly decreases the plastic viscosity by 2%. The modification of cement paste by MWCNT changes the shear thinning index from 0.70 to 0.64.

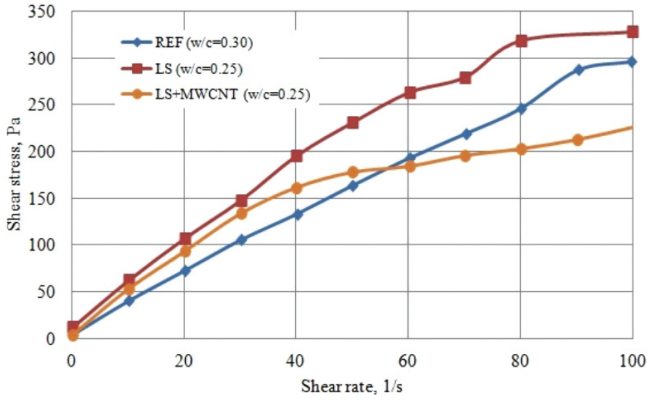

Fig. 5 Flow curves of cement paste with and without MWCNT in the presence of LS in 5 min after cement paste mixing
5. ábra A cementpép folyási görbéi MWCNT-vel és anélkül LS jelenlétében 5 perc alatt a cementpép keverése után

The cement paste modified by MWCNT in the presence of NF plasticizer characterized by the increase of yield stress and plastic viscosity by 4% and 20%, respectively. The shear thinning was changed from 0.83 for cement paste modified by NF to 0.74 for cement paste with MWCNT and NF. The flow curves of cement pastes modified by MWCNT in the presence of NF are represented in *Fig. 6*.

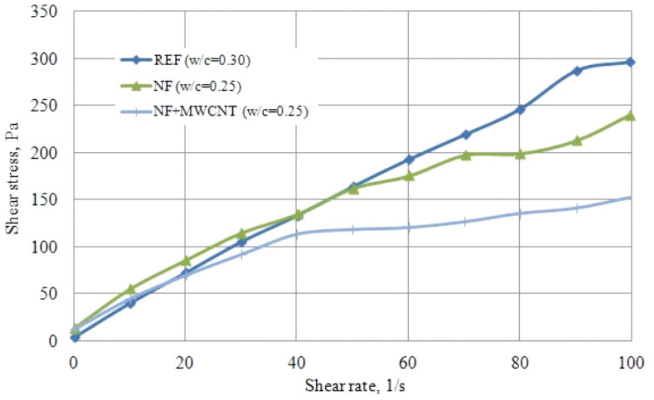

Fig. 6 Flow curves of cement paste with and without MWCNT in the presence of NF in 5 min after cement paste mixing
6. ábra A cementpép folyási görbéi MWCNT-vel és anélkül NF jelenlétében 5 perc alatt a cementpép keverése után

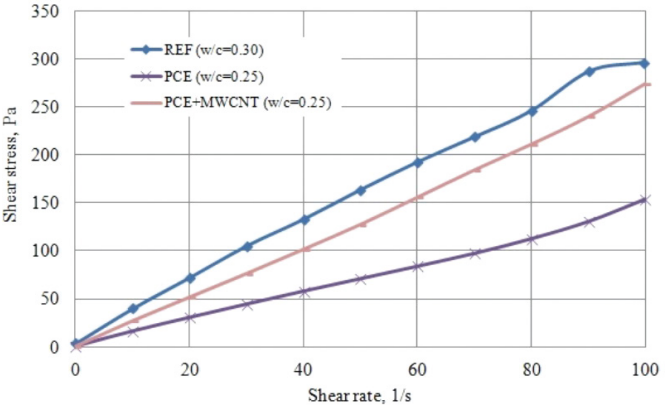

Fig. 7 Flow curves of cement paste with and without MWCNT in the presence of PCE in 5 min after cement paste mixing
7. ábra A cementpép folyási görbéi MWCNT-vel és anélkül PCE jelenlétében 5 perc alatt a cementpép keverése után

The remarkable changes in rheological parameters of cement pastes were observed in case of their modification by MWCNT in the presence of PCE plasticizer. The flow curves of cement paste modified by MWCNT in the presence of PCE plasticizer are shown in *Fig. 7*. The addition of MWCNT to cement paste with PCE plasticizer led to the increase of the yield stress by 33% in comparison with cement paste modified only by PCE plasticizer. The plastic viscosity of nano modified cement paste increased in 2 times in comparison with cement paste with PCE plasticizer. The cement paste with PCE plasticizer characterized by shear thickening flow behaviour. The modification by MWCNT decreased the shear thickening index from 1.20 to 1.18.

The absolute values of tested rheological parameters of cement paste with MWCNT in the presence of LS, NF and PCE plasticizers are given in *Table 2*.

Specimen	W/C ratio	τ_0, Pa	K, Pa·s^n	n
Reference	0.30	3.6	4.0	0.94
MWCNT	0.30	3.9	4.2	0.98
LS	0.25	11.4	13.5	0.70
LS+MWCNT	0.25	12.0	13.3	0.64
NF	0.25	5.2	6.0	0.83
NF+MWCNT	0.25	5.4	4.8	0.74
PCE	0.25	0.3	0.6	1.20
PCE+MWCNT	0.25	0.4	1.2	1.18

Table 2 Rheological parameters of cement pastes with and without MWCNT in presence of plasticizing admixtures obtained based on Herschel-Bulkley model
2. táblázat A cementpépek reológiai paraméterei MWCNT-vel vagy anélkül folyósítószerek jelenlétében a Herschel-Bulkley modell alapján

MWCNT has an impact on the rheological properties of cement pastes. The small size, high aspect ratio, specific surface and porous structure of MWCNT can be a reason for the observed influence on the cement paste. These features of MWCNT contribute them to act physically and chemically in the cement paste. The usage of MWCNT in combination with various polymer PL can increase or decrease their impact on the rheological properties of the cement pastes in dependence on the chemical structure of PL and its ability to interact with MWCNT.

4. Discussions of results

As it was mentioned above, the Herschel-Bulkley and modified Bingham rheological models give more information about the rheological behaviour of the studied cement systems [16-23].

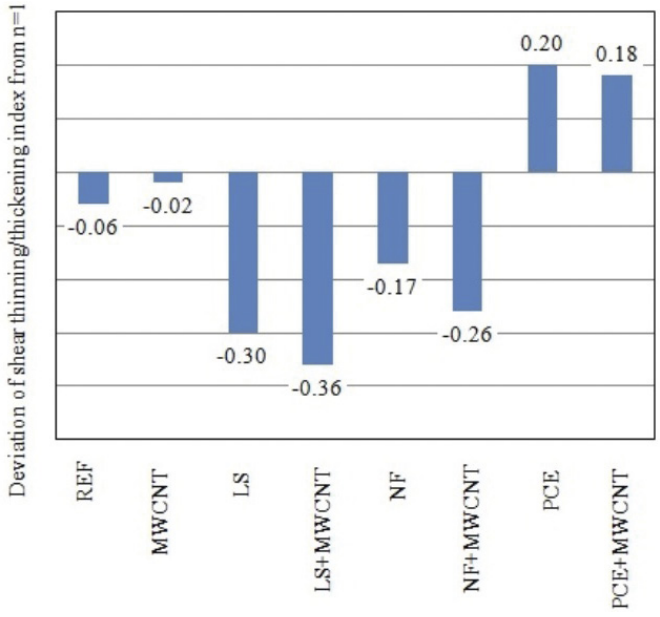

Fig. 8 Deviation of shear thinning/thickening indexes from n=1 in absolute units
8. ábra A nyírási vékonyodási / vastagodási indexek eltérése n = 1-től abszolút egységekben

In the course of the present research, the approximation of the rheological flow curves by Herschel Bulkley model identified the changes of shear thinning/thickening indexes for cement pastes modified by MWCNT in the presence of PL. The shear thinning indexes for cement pastes with MWCNT in the presence of LS and NF were changed from 0.70 to 0.64 and from 0.83 to 0.74, respectively. The cement pastes with MWCNT in the presence of PCE plasticizer were characterized by the changes of shear thickening index from 1.20 to 1.18. The *Fig. 8* presents the deviation of the pseudoplastic indexes of cement pastes from n=1 in absolute units.

Based on the obtained results, it can be concluded that the addition of MWCNT to cement paste in the presence of various polymer PL leads to the decrease of dilatancy of cement paste. The level of changes in pseudoplastic index is depended on the type of applied PL and can be explained by its molecular structure.

5. Conclusions

1. The cement pastes have non-linear rheological behaviour. The processing of rheological data based on non-linear Herschel-Bulkley or Bingham rheological models allows obtaining more rheological parameters with high accuracy.

2. The various types of polymer plasticizing admixtures have a different influence on the cement paste flow behaviour. The application of LS, NF increases the thixotropy of cement pastes. The usage of PCE plasticizer revealed the increase of dilatancy of cement paste in comparison with the reference sample without admixtures.

3. The MWCNT have an impact on the rheological parameters of cement paste. The complex usage of MWCNT with LS and NF revealed the increase of yield stress by 5 and 4%, respectively. The plastic viscosity decreased by 2% in case of a modification of cement paste by MWCNT and LS. The usage of MWCNT with NF plasticizer led to an increase of the plastic viscosity of the cement paste by 20%. The more significant changes in rheological parameters of cement pastes were obtained for cement pastes modified by MWCNT in the presence of PCE plasticizer. The yield stress increased by 33% and plastic viscosity enhanced in 2 times in comparison with cement paste without MWCNT. The evaluation of shear thinning/ thickening indexes of nanomodified cement pastes identified that MWCNT contribute to the decrease of dilatancy of cement pastes. The observed differences in rheological behaviour of nanomodified cement paste in the presence of different plasticizing admixture can be explained by physical and chemical interactions between polymers and MWCNT.

4. Modification by MWCNT allows obtaining the cement paste of low dilatancy with definite flowability, yield stress and viscosity.

References

[1] Secrieru, E. – Cotardo, D. – Mechtcherine, V. – Lohaus, L. – Schrofl, C. – Begemann, C. (2018): Changes in concrete properties during pumping and formation of lubricating material under pressure. Cement and Concrete Research. Vol. 108, pp. 129–139, https://doi.org/10.1016/j.cemconres.2018.03.018

[2] Kim, J. H. – Kwon, S. H. – Kawashima, S. – Yim, H. J. (2017): Rheology of cement paste under high pressure. Cement and Concrete Composites. Vol. 77, pp. 60-67, https://doi.org/10.1016/j.cemconcomp.2016.11.007

[3] Nerella, V. N. – Mechtcherine, V. (2018): Virtual Sliding Pipe Rheometer for estimating pumpability of concrete. Construction and Building Materials. Vol. 170, pp. 366–377, https://doi.org/10.1016/j.conbuildmat.2018.03.003

[4] Xie, H. – Liu, F. – Fana, Y. – Yang, H. – Chen, J. – Zhang, J. – Zuo, C. (2013): Workability and proportion design of pumping concrete based on rheological parameters. Construction and Building Materials. Vol. 44, pp. 267–275, https://doi.org/10.1016/j.conbuildmat.2013.02.051

[5] Kim, J. S. – Kwon, S. H. – Jang, K. P. – Choi, M. S. (2018): Concrete pumping prediction considering different measurement of the rheological properties. Construction and Building Materials, Vol. 171, pp. 493–503, https://doi.org/10.1016/j.conbuildmat.2018.03.194

[6] Wallevik, J. E. – Wallevik, O. H. (2020): Concrete mixing truck as a rheometer. Cement and Concrete Research, Vol. 127, 105930, https://doi.org/10.1016/j.cemconres.2019.105930

[7] Megid, W. A. – Khayat, K. H. (2018): Effect of concrete rheological properties on quality of formed surfaces cast with self-consolidating concrete and superworkable concrete. Cement and Concrete Composites, Vol. 93, pp. 75–84, https://doi.org/10.1016/j.cemconcomp.2018.06.016

[8] Kostrzanowska-Siedlarz, A. – Jacek Gołaszewski, J. (2016): Rheological properties of High Performance Self-Compacting Concrete: Effects of composition and time. Construction and Building Materials, Vol. 115, pp. 705–715, https://doi.org/10.1016/j.conbuildmat.2016.04.027

[9] Iris, G.-T. – Belen, G.-F. – Fernando, M.-A. – Diego, C.-L. (2017): Self-compacting recycled concrete: Relationships between empirical and rheological parameters and proposal of a workability box. Construction and Building Materials, Vol. 143, pp. 537–546, https://doi.org/10.1016/j.conbuildmat.2017.03.156

[10] Paul, S. C. – Tay, Y. W. D. – Panda, B. – Tan M. J. (2018): Fresh and hardened properties of 3D printable cementitious materials for building and construction. Archives of Civil and Mechanical Engineering, Vol. 18, pp. 311-319, https://doi.org/10.1016/j.acme.2017.02.008

[11] Weng, Y. – Li, M. – Tan, M. J. – Qian, S. (2018): Design 3D printing cementitious materials via Fuller Thompson theory and Marson-Percy model. Construction and Building Materials, Vol. 163, pp. 600–610, https://doi.org/10.1016/j.conbuildmat.2017.12.112

[12] Lu, B. – Qian, Y. – Li, M. – Weng, Y. – Leong, K. F. – Tan, M. J. – Qian, S. (2019): Designing spray-based 3D printable cementitious materials with fly ash cenosphere and air entraining agent. Construction and Building Materials, Vol. 211, pp. 1073–1084, https://doi.org/10.1016/j.conbuildmat.2019.03.186

[13] Gram, A. – Silfwerbrand, J. – Lagerblad, B. (2014): Obtaining rheological parameters from flow test — Analytical, computational and lab test approach. Cement and Concrete Research, Vol. 63, pp. 29–34, https://doi.org/10.1016/j.cemconres.2014.03.012

[14] Skripkiunas, G. – Karpova, E. – Barauskas, I. – Bendoraitiene, J. – Yakovlev, G. (2018): Rheological Properties of Cement Pastes with Multiwalled Carbon Nanotubes. Advances in Materials Science and Engineering, Vol. 2018, Article ID 8963542, pp.1-13, https://doi.org/10.1155/2018/8963542

[15] Macijauskas, M. – Girskas, G. (2017): The Influence of Commonly Used Plasticizing Admixtures on the Plasticizing Effect of Cement Paste. Construction Science, Vol. 20, pp. 26-32, https://doi.org/10.2478/cons-2017-0004

[16] Feys, D. – Wallevik, J. E. – Yahia, A. – Khayat, K. H. – Wallevik, O. H. (2013): Extension of the Reiner–Riwlin equation to determine modified Bingham parameters measured in coaxial cylinders rheometers. Materials and Structures, Vol. 46, pp. 289–311, https://link.springer.com/article/10.1617/s11527-012-9902-6

[17] Ma, S. – Qian, Y. – Kawashima, S. (2018): Experimental and modeling study on the non-linear structural build-up of fresh cement pastes incorporating viscosity modifying admixtures. Cement and Concrete Research, Vol. 108, pp. 1–9, https://doi.org/10.1016/j.cemconres.2018.02.022

[18] Guneyisi, E. – Gesoglu, M. – Algın, Z. – Yazıcı, H. (2016): Rheological and fresh properties of self-compacting concretes containing coarse and fine recycled concrete aggregates. Construction and Building Materials, Vol. 113, pp. 622–630, https://doi.org/10.1016/j.conbuildmat.2016.03.073

[19] Nguyen, V. H. – Remond, S. – Gallias, J. L. – Bigas, J. P. – Muller, P. (2006): Flow of Herschel–Bulkley fluids through the Marsh cone. J. Non-Newtonian Fluid Mech., Vol. 139, pp. 128–134, https://doi.org/10.1016/j.jnnfm.2006.07.009

[20] Khayat, K. H. – Meng, W. – Vallurupalli, K. – Teng, L. (2019): Rheological properties of ultra-high-performance concrete — An overview. Cement and Concrete Research, Vol. 124, 105828, https://doi.org/10.1016/j.cemconres.2019.105828

[21] Yahia, A. (2011): Shear-thickening behavior of high-performance cement grouts — Influencing mix-design parameters. Cement and Concrete Research, Vol. 41, pp. 230–235, https://doi.org/10.1016/j.cemconres.2010.11.004

[22] Reales, O. A. M. – Jaramillo, Y. P. A. – Botero, J. C. O. – Delgado, C. A. – Quintero, J. H. – Filho, R. D. T. (2018): Influence of MWCNT/surfactant dispersions on the rheology of Portland cement pastes. Cement and Concrete Research, Vol. 107, pp. 101–109, https://doi.org/10.1016/j.cemconres.2018.02.020

[23] Jiang, S. – Shan, B. – Ouyang, J. – Zhang, W. – Yu, X. – Li, P. – Han, B. (2018): Rheological properties of cementitious composites with nano/fiber fillers. Construction and Building Materials, Vol. 158, pp. 786–800, https://doi.org/10.1016/j.conbuildmat.2017.10.072

Ref.:
Skripkiunas, G. – **Karpova,** E. – **Dauksys, M.**: *Rheological behaviour modelling of cement paste with nanotubes and plasticizer*
Építőanyag – Journal of Silicate Based and Composite Materials, Vol. 71, No. 6 (2019), 184–189. p.
https://doi.org/10.14382/epitoanyag-jsbcm.2019.32

Sol-gel synthesis and structural characterization of Fe doped barium titanate nanoceramics

Mohammed TIHTIH ▪ Institute of Ceramics and Polymer Engineering, University of Miskolc, Hungary ▪ medtihtih@gmail.com

Karoum LIMAME ▪ Laboratoire de Physique Théorique et Appliquée, Morocco ▪ klimame1974@yahoo.com

Yahya ABABOU ▪ Laboratoire de Physique Théorique et Appliquée, Morocco ▪ Ababou.yahya0@hotmail.com

Salaheddine SAYOURI ▪ Laboratoire de Physique Théorique et Appliquée, Morocco ▪ s.sayouri12@gmail.com

Jamal-Eldin F. M. IBRAHIM ▪ Institute of Ceramics and Polymer Engineering, University of Miskolc, Hungary ▪ jamalfadoul@gmail.com

Érkezett: 2019. 11. 29. ▪ Received: 29. 11. 2019. ▪ https://doi.org/10.14382/epitoanyag-jsbcm.2019.33

Abstract

Fe-doped barium titanate (BFe_xT) nanoceramics were successfully prepared by a simple sol-gel process, these materials are very interesting and could be a candidate for many optoelectronic applications. X-ray diffraction (XRD) patterns of the obtained samples, heat-treated at a quite low temperature (800 °C/3h) revealed that BFe_xT nanoceramics crystallized into a tetragonal phase perovskite structure. The occupation of the Ba and Ti sites by Fe in the $BaTiO_3$ lattice and the evolution of the different parameters (crystallite size, lattice parameters and strain) as functions of the Fe doping have been discussed in details using several characterization techniques including XRD and Fourier Transformation Infrared (FT-IR).

Keywords: Sol-gel, Barium titanate nanoceramics, Fe-doped barium titanate nanoceramics, X-ray Diffraction

Kulcsszavak: Szol-gél, bárium-titanát, nanokerámia, Fe-adalékolt bárium-titanát, röntgendiffrakció

Mohammed TIHTIH
Is a lecturer in the Sidi Mohamed Ben abdellah University, Morocco, he graduated from Faculty of sciences Dhar El Mahraz, Fez, Morocco, Department of Physics, for the time being, he is a PhD student in the University of Miskolc, Institute of Ceramics and Polymer Engineering, under supervision of Prof. L. A. Gömze

Karoum LIMAME
Lecturer and Researcher, research interests: Synthesis and Processing of Ceramics and Compounds, Materials Characterization and Simulation for the teaching of physics Work Experience: Titular Researcher, at "Sidi Mohamed Ben Abdellah University" publications in JCR Journals in the field of Ceramics Materials and Composites.

Yahya ABABOU
is establisher and professor of the Department of physics in the Faculty of Sciences Dhar El mahraz Sidi Mohamed Ben Abdellah University, Morocco.

Salaheddine SAYOURI
is professor and Head of Laboratory of Theoretical and Applied Physics, Department of Physics, Sidi Mohamed Ben Abdellah University. Author and co-author of 4 patents and more than 90 scientific articles indexed Scopus.

Jamal-Eldin F. M. IBRAHIM
is a lecturer in the University of Bahri, Khartoum, Sudan, he graduated from University of Marmara, Istanbul, Turkey, Institute of Pure and Applied Sciences, Department of Metallurgical and Materials Engineering, for the time being, he is a PhD student in the University of Miskolc, Institute of Ceramics and Polymer Engineering, under supervision of Prof. L. A. Gömze

1. Introduction

The popularity of the research in the area of the high-tech ceramics is largely grown lately [1-31], since the discovery of the ferroelectricity phenomenon, barium titanate $BaTiO_3$ (BT) has been a fundamental member of the ferroelectric perovskite family. This compound has been used for a long time in many industrial sectors including full swing multilayer ceramic capacitors (MLCCs) [32], the realization of the ferroelectric random access memories (FRAMs) [33], thermistors manufacturing [34] and detection of polluting gases such as CO [35]. However, multilayer capacitors have long been at the forefront of $BaTiO_3$ applications. The $BaTiO_3$ nanoceramics can be synthesized by various methods such as solid-state reaction [36], hydrothermal synthesis [37], sol-gel [38] and co-precipitation method [39], compared to other methods, sol-gel is considered as a simple and easy method which can allows production of a high purity $BaTiO_3$ with very fine particles of controllable size, moreover, it is possible to easily modify the physical properties of BT since these are very sensitive to doping on the A-site (Ba_DTiO_3), B-site ($BaTi_DO_3$) and substitution on both sites (co-doping) $Ba_DTi_{D'}O_3$ which mainly depends on their ionic radii [40]. Recently, the doping of $BaTiO_3$ nanoceramics by 3d transition metals (Fe, Co, Mn, Ni...) have attracted much attention, 3d transition elements are more likely to be considered as dopants due to their electric and high magnetic properties. To date, a number of research works have reported the effect of the 3d transition metals on the structural and physicochemical properties of $BaTiO_3$ nanoceramics. Rani et al [41] have studied the effect of Fe doping on structural, magnetic and magnetoelectric properties of $BaTiO_3$ prepared via solid-state reaction route. Khirade et al [42] have reported the effect of Fe doping on the structural, optical and electrical properties of $BaTiO_3$ nanoceramics synthesis by sol-gel process. Maikhuri et al [43] have demonstrated the influence of A- and B-site substitution on the structural and magnetic properties of $BaTiO_3$. In the present work, Fe doped $BaTiO_3$ nanoceramics have been prepared using sol-gel method, the prepared samples were characterized using X-Ray Diffraction and FT-IR. The analysis of X-ray patterns was used to calculate the crystallite size, lattice parameters and lattice strain. The aim of this investigation is to study the effect of Fe dopant on the structural properties of $BaTiO_3$, In particular, the occupation of Ba and/or Ti sites by Fe in the $BaTiO_3$ structure.

2. Method of elaboration

Pure and Fe-doped $BaTiO_3$ were synthesized using sol-gel method, barium acetate trihydrate ($Ba(CH_3CO_2)_2.3H_2O$), Iron acetate $Fe(C_2H_3O_2)_2$ and titanium alkoxide $Ti[OCH(CH_3)_2]_4$ were used as precursors, lactic acid (CH_3CH (OH)COOH) was used as peptizing agent, acetic acid was added to dissolve Iron acetate, and distilled water as solvent. As shown in *Fig. 1*, the first step is to prepare a colloidal solution of TiO_2, to do this; the

titanium alkoxide was added to an aqueous solution of lactic acid and H_2O with continuous stirring at 70 °C. After 24 hours of reaction, the white precipitate obtained is changed into a clear homogeneous solution. In a second step, the colloidal solution produced was added in stoichiometric quantities to iron and barium acetates. The obtained transparent sol was converted to a translucent gel after stirring at 90 °C. Fine powders were prepared from the gel after drying at 90 °C and grinding. Finally, the nanopowders produced were calcined in air at a temperature of 800 °C for 3 h in a programmable oven. Phase identification of the prepared BFexT was performed using X-ray diffraction (Cu Kα radiation, λ = 1.5405980 Å) and Fourier transform infrared.

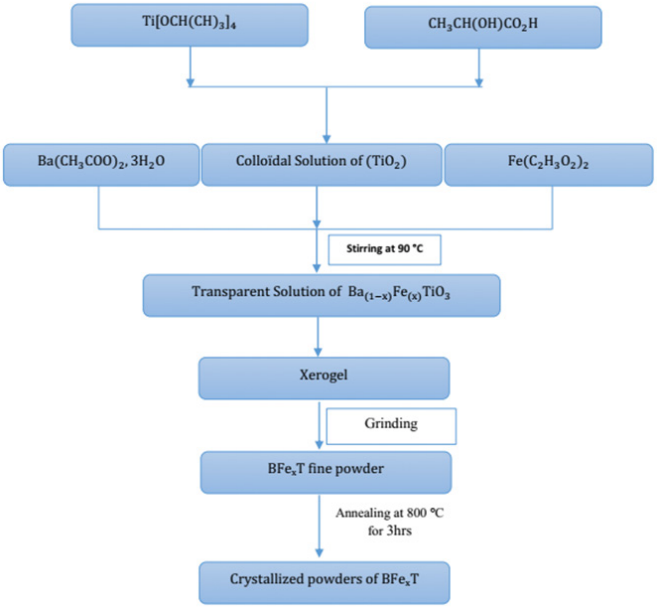

Fig. 1 *Flow chart of the preparation of Fe doped $BaTiO_3$ nanoceramics by sol-gel process*
1. ábra *A Fe-adalékolt $BaTiO_3$ nanokerámia szol-gél eljárással történő előállításának folyamatábrája*

3. Results and discussion

3.1 Structural studies

Fig. 2 shows the X-ray diffraction patterns of $Ba_{1-x}Fe_xTiO_3$ (x = 0, 1, 3%) samples prepared via sol-gel method. XRD patterns of pure and Fe-doped $BaTiO_3$ show a single tetragonal phase without any evidence of secondary phases. The XRD pattern of the samples can be indexed to the tetragonal perovskite structure with P4mm space group, which is in great concurrence with JCPDS No. 05-0626. An important fact revealed in *Fig. 2* is that the peak of (101) of $Ba_{1-x}Fe_xTiO_3$ (x=0.01) is shifted to higher 2θ angle compared to the pure $BaTiO_3$, while the peak of (101) of $Ba_{1-x}Fe_xTiO_3$ (x=0.03) is shifted to lower 2θ angle. The Peaks shifted to lower and higher angles indicate an increase and decrease in volume (V) of the unit cell respectively as shown in *Table 1*. Fe^{2+} has a smaller ionic radius (0.78 Å) compared to that of Ba^{2+} (1.35 Å). The slight shift of the peak positions in BFe1T with respect to $BaTiO_3$ is may be attributed to the Fe^{2+} ionic size difference, which could eventually replace the Ba^{2+} ions in the $BaTiO_3$ lattice [40] and leads to a reduction in the volume of the unit cell. In addition, the lower angle shift in the peaks of BFe3T can be assigned to the substitution of Fe^{2+} ion by Ba^{2+} and Ti^{4+} ions, but with a predominance of the Ti site occupancy in the $BaTiO_3$ lattice. In contrary, and because of the reason that the Fe^{2+} ionic radii is larger compared to Ti^{4+} (0.605 Å), it can be observed that the substitution of Ti-sites by Fe^{2+} create oxygen vacancies to neutralize the charge. Therefore, an increase in the unit cell volume is predicted as the unit cell parameters a and c have increased.

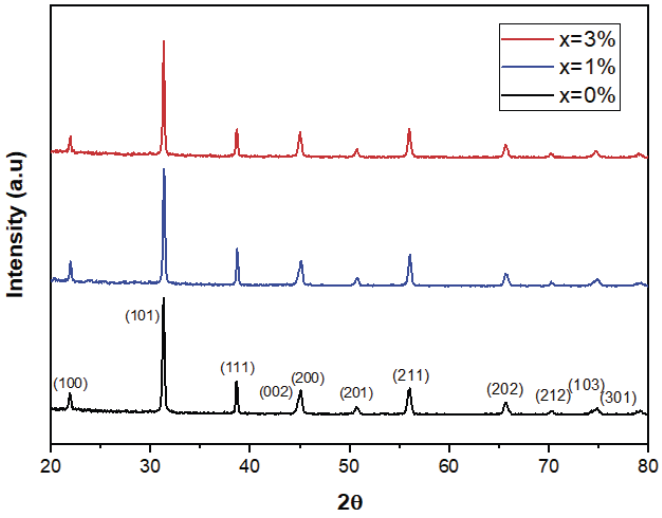

Fig. 2 *X-ray diffraction patterns of prepared Fe-doped barium titanate nanoceramics*
2. ábra *Az elkészített Fe-adalékolt bárium-titanát nanokerámiák röntgendiffraktogramja*

The crystallite size of the pure and Fe-doped $BaTiO_3$ was calculated from the X-ray diffraction patterns according to (101) peak using Debye-Scherrer formula [44]:

$$D = \frac{0.9\lambda}{\beta \cos\theta} \quad (1)$$

Where D is the crystallite size, λ is x-ray wavelength, θ is the diffraction angle and β is full width at half maximum (FWHM) of the (101) peak. The average crystallite size was calculated by settling the highest intensity peak. As listed in *Table 1*.

Moreover, the lattice strain (ε) of all samples was estimated using the following equation [45]:

$$\varepsilon = \frac{\beta}{4\tan\theta} \quad (2)$$

The estimated lattice parameters a and c, unit cell volume (V), position of the peak (101), lattice strain and crystallite size are listed in *Table 1*. It was found that the average crystallite size (D) increased with Fe concentration x. However, the lattice constant (c) and lattice strain have been decreased after doping. The increase in crystallite size is due to the big difference between the ionic radius of Fe^{2+}, Ba^{2+} and Ti^{4+} [31, 42]. The shift in the position of (101) in the XRD patterns and the change in the volume of unit cell after doping reveal that Fe is totally soluble into $BaTiO_3$ lattice.

3.2 FT-IR analysis

The Fourier transform infrared spectroscopy (FT-IR) spectrums of $BaFe_xTiO_3$ (x=0, 1, 3%) are shown in *Fig. 3*. The corresponding spectra show absorption bands in the wave number ranging from 4000 – 450 cm^{-1}. The presence of a prominent peak at about 500 cm^{-1} in the pure $BaTiO_3$ spectrum corresponds to the vibration of Ti-O bond in the crystal lattice [46]. All the samples show a fingerprint of Ti-O and Ti-O-Ti bonds between 500 cm^{-1} and 750 cm^{-1} which is a molecular fingerprint of $BaTiO_3$. The wavenumber of the absorption peak of Ti–O bond increases after doping, the peak is shifted from 481.12 cm^{-1} in pure $BaTiO_3$ to 491.23 cm^{-1} in 3% Fe doped $BaTiO_3$ which indicates the change of the unit cell size. Moreover, the bands observed in the region from 1425 cm^{-1} to 1449 cm^{-1} could be attributed to $BaCO_3$ phase present in the prepared samples [47].

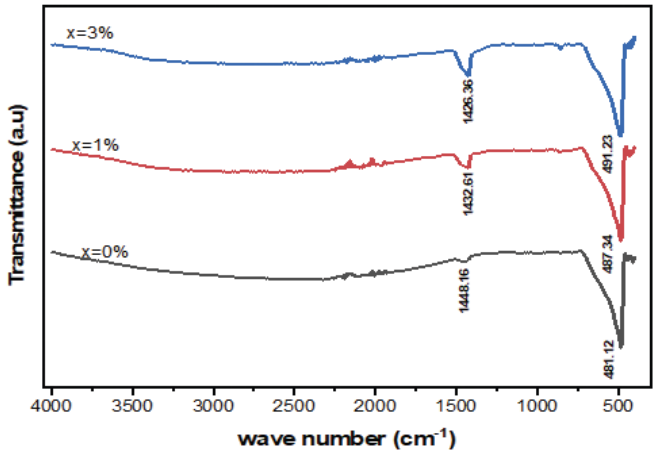

Fig. 3 FT-IR spectrums of pure and Fe-doped barium titanate at different Concentrations (x=0, 0.01 and 0.03)
3. ábra A tiszta és a Fe-adalékolt bárium-titanát FT-IR spektrumai különböző koncentráció esetén (x=0; 0,01 és 0,03)

x	a (Å)	c (Å)	V (Å³)	Position 2Θ of (101)	Crystallite size (nm)	Lattice strain
0	3.9943	4.0191	64.12245	31.31533	34.56	0.003883
0.01	3.9949	4.0164	64.01643	31.36792	36.38	0.003584
0.03	4.0013	4.0167	64.30898	31.33112	42.46	0.003159

Table 1 The position of the peak (101), lattice parameters, Volume of the unit cell, lattice strain and crystallite size of $BaFe_xTiO_3$ (x=0, 1 and 3%) nanoceramics
1. táblázat A csúcs helyzete (101), a rácsparaméterek, az egységcellák térfogata, a rácsos törzs és a $BaFe_xTiO_3$ (x=0; 1 és 3%) nanokerámia kristálymérete

4. Conclusion

To summarize, pure and Fe doped barium titanate nanoceramics were synthesized using sol-gel method, the obtained powders were calcined at 800 °C for 3h, the calcined samples were characterized using XRD and FT-IR spectroscopy. The XRD results confirm the presence of single tetragonal phase for both pure and Fe doped materials. This measurement reveals that the Fe^{2+} ion may replace Ba^{2+} for x=1% or the both Ba^{2+} and Ti^{4+} but with a predominance for the Ti-site in the case of x=3%. FT-IR measurements showed that the elaborated samples have perovskite structure, which is in a good agreement with XRD results. The modification in the structural properties after doping indicates that Fe has successfully doped into $BaTiO_3$ lattice.

Acknowledgements

Thanks to the University of Miskolc (Hungary), University Sidi Mohamed Ben Abdellah USMBA (Morocco) to support this work.

References

[1] Emese Kurovics et al (2019): Effect of composition and heat treatment on porosity and microstructures of technical ceramics made from kaolin and IG-017 additive, IOP Conf. Ser.: Mater. Sci. Eng.vol. 613 012025 https://doi.org/10.1088/1757-899X/613/1/012025
[3] J. F. M. Ibrahim et al (2019): The Influence of Cr doping on the Structural and Magnetic Properties of HoMnO3 Multiferroic Ceramics, IOP Conf. Ser.: Mater. Sci. Eng. Vol. 613 012009 https://doi.org/10.1088/1757-899X/613/1/012009
[3] Gömze, László A. – Ludmila N. Gömze (2003): *Építőanyag–JSBCM* vol. 55 no. 4 pp. 133-140 http://dx.doi.org/10.14382/epitoanyag-jsbcm.2003.23
[4] Gömze, L. A. – Gömze, L. N. (2013): Ceramic based lightweight composites with extreme dynamic strength, *IOP Conf. Ser.: Mater. Sci. Eng.* Vol. 47 012033 https://doi.org/10.1088/1757-899X/47/1/012033
[5] Gömze, L. A., 2016: Applied materials science I. *Compilation of Selected Scientific Papers*, pp.1-189.
[6] Gömze, L. A. – Gömze, L. N. (2011): "Hetero-modulus alumina matrix nanoceramics and CMCs with extreme dynamic strength" *IOP Conf. Ser.: Mater. Sci. Eng. Vol.* 18 082001 http://dx.doi.org/10.1088/1757-899X/18/8/082001
[7] Gömze, L. A. – Gömze, L. N. (2017): Rheological principles of development hetero-modulus and hetero-viscous complex materials with extreme dynamic strength, *IOP Conf. Ser.: Mater. Sci. Eng. Vol.* 175 012001 http://dx.doi.org/10.1088/1757-899X/175/1/012001
[8] Gömze, L. A. – Gömze, L. N. (2010): Mechanical stress relaxation in hetero-modulus, hetero-viscous complex ceramic materials, Építőanyag–*JSBCM vol.* 62 no. 4 p. 98 http://dx.doi.org/10.14382/epitoanyag-jsbcm.2010.18
[9] E. Kurovics et al (2017): Development ceramic composites based on Al_2O_3, SiO_2 and IG-017 additive, IOP Conf. Ser.: Mater. Sci. Eng. Vol. 175 012013 https://doi.org/10.1088/1757-899X/175/1/012013
[10] Gömze, L. A. – Gömze, L. N. (2009): Alumina-based hetero-modulus ceramic composites with extreme dynamic strength – phase transformation of Si3N4 during high speed collisions with metallic bodies, Építőanyag–JSBCM vol. 61 no. 2 p. 38 http://dx.doi.org/10.14382/epitoanyag-jsbcm.2009.7
[11] Kulkov, S. N. – Savchenko, N. L. (2008): Wear behavior of zirconia-bazed ceramics under high-speed dry sliding on steel, Építőanyag–JSBCM vol. 60 no. 3 pp. 62-65. http://dx.doi.org/10.14382/epitoanyag-jsbcm.2008.10
[12] J. F. M. Ibrahim et al (2019): The influence of composition, microstructure and firing temperature on the density, porosity, and shrinkage of new zeolite-alumina composite material, Építőanyag–JSBCM vol. 71 no. 4 p. 120 https://doi.org/10.14382/epitoanyag-jsbcm.2019.21
[13] O. B. Kotova, et al (2019): Composite materials based on zeolite-montmorillonite rocks and aluminosilicate wastes, Építőanyag–JSBCM vol. 71 no. 4 p. 125 https://doi.org/10.14382/epitoanyag-jsbcm.2019.22
[14] E. Kurovics, et al (2019): Composite materials based on zeolite-montmorillonite rocks and aluminosilicate wastes, Építőanyag–JSBCM vol. 71 no. 4 p. 114 https://doi.org/10.14382/epitoanyag-jsbcm.2019.20
[15] T. Shchemelinina et al (2019): Clay- and zeolite-based biogeosorbents: modelling and properties, Építőanyag–JSBCM vol. 71 no. 4 p. 131 https://doi.org/10.14382/epitoanyag-jsbcm.2019.23
[16] Gömze, L. A. – Kulkov, S. N. – Kurovics, E. – Buyakov, A. S. – Buzimov, A. Y. – Grigoriev, M. V. – Kanev, B. I. – Kolmakova, T. V. – Levkov, R. V. – Sitkevich, S. A. (2018): Development ceramic floor tiles with increased

shear and pressure strengths, Építőanyag–JSBCM vol. 70 no. 1 p. 13 https://doi.org/10.14382/epitoanyag-jsbcm.2018.3

[17] Kurovics, E. – Buzimov, A. Y. – Gömze, L. A. (2016): Influence of raw materials composition on firing shrinkage, porosity, heat conductivity and microstructure of ceramic tiles, IOP Conf. Ser.: Mater. Sci. Eng. Vol. 123, No. 1, p. 012058 https://doi.org/10.1088/1757-899X/123/1/012058

[18] Khare, S. – Sharma, M. – Venkateswarlu, K. (2010): Effect of scandium additions on pressure less sintering of Al-TiN metal matrix composites, Építőanyag–JSBCM vol. 62 no. 2 p. 39. http://dx.doi.org/10.14382/epitoanyag-jsbcm.2010.8

[19] Ershova, N. I. – Kelina, I. Y. (2009): High-temperature wear-resistant materials based on silicon nitride , Építőanyag - JSBCM vol. 61 no. 2 pp. 34-37. http://dx.doi.org/10.14382/epitoanyag-jsbcm.2009.6

[20] Miranda-Hernandez, J. G. – La Torre, D. – Diaz, S. – Rocha-Rangel, E. (2010): Synthesis, microstructural analysis and mechanical properties of alumina-matrix cermets, Építőanyag - JSBCM vol. 61 no. 1 pp.1-5. http://dx.doi.org/10.14382/epitoanyag-jsbcm.2010.1

[21] Apkaryan, A. S. – Kulkov, S. N. – Gömze, L. A. (2014): Foam Glass Ceramics as Composite Granulated Heat-Insulating Material, Építőanyag–JSBCM vol. 66 no. 2 pp. 38-42. http://dx.doi.org/10.14382/epitoanyag-jsbcm.2014.8

[22] Lebedeva, N. N. – Orbukh, V. I. – Eyvazova, G. M. – Darvishov, N. H. – Akhundov, C. G. (2018): Mass transfer of aluminum film from the surface of zeolite on the cathode, Építőanyag–JSBCM vol. 70 no. 4 p. 120 https://doi.org/10.14382/epitoanyag-jsbcm.2018.22

[23] A. Buyakov et al (2019): Structure and mechanical properties of ZrO2-MgO composites with bimodal pore structure, IOP Conf. Ser.: Mater. Sci. Eng. Vol. 613 012023 https://doi.org/10.1088/1757-899X/613/1/012023

[24] László A. Gömze et al (2019): Conventional Brick Clays as a Challenge of Materials Science – New Explanation of Drying Sensitivities, IOP Conf. Ser.: Mater. Sci. Eng. Vol. 613 012005 https://doi.org/10.1088/1757-899X/613/1/012005

[25] Yu A Rikun et al (2019): Computer Modeling of the Stress-Strain State of the Cervical Spine Segment, IOP Conf. Ser.: Mater. Sci. Eng. Vol. 613 012027 https://doi.org/10.1088/1757-899X/613/1/012027

[26] S .N. Kulkov (2019): Smart Materials Based on a High and Low Temperatures SME-Alloys, IOP Conf. Ser.: Mater. Sci. Eng. Vol. 613 012002 https://doi.org/10.1088/1757-899X/613/1/012002

[27] A Hamza et al (2019): Plasticity of Red Mud and Clay Mixtures, IOP Conf. Ser.: Mater. Sci. Eng. Vol. 613 012051 https://doi.org/10.1088/1757-899X/613/1/012051

[28] L. A. Gömze et al (2013) Comparison of material structures and scratch strength of thin films of glass mirrors and automobile windscreens, IOP Conf. Ser.: Mater. Sci. Eng. Vol. 47 012023 https://doi.org/10.1088/1757-899X/47/1/012023

[29] S. Kulkov (2013): Formation of Nanostructures in Brittle Materials with Transformations, IOP Conf. Ser.: Mater. Sci. Eng. Vol. 47 012042 https://doi.org/10.1088/1757-899X/47/1/012042

[30] A. Y. Buzimov et al (2017): Influence of mechanical activation on the properties of natural zeolites from Tokaj Mountain, IOP Conf. Ser.: Mater. Sci. Eng. Vol. 175 012033 https://doi.org/10.1088/1757-899X/175/1/012033

[31] A. Shmakova et al (2017): Crystal chemical characteristics and physical properties of ferrous minerals as the basis for the formation of functional materials, IOP Conf. Ser.: Mater. Sci. Eng. Vol. 175 012015 https://doi.org/10.1088/1757-899X/175/1/012015

[32] A. A. Wereszczak – K. Breder – M. K Ferber, – R. J. Bridge – L. Riester – T. P Kirkland 1998 (No. ORNL/CP-98893; CONF-980521-). Oak Ridge National Lab., TN (United States). https://doi.org/10.2172/290938

[33] J. F. Scott (2005) New developments on FRAMs: [3D] structures and all-perovskite FETs, Materials Science and Engineering: B vol. 120 no. 1-3 p. 6 https://doi.org/10.1016/j.mseb.2005.02.047

[34] D. Zhou, – Y. Chen, – D. Zhang, – H. Liu, – Y. Hu – S. Gong (2004) Fabrication and characterization of the multilayered PTCR ceramic thermistors by slip casting, *Sensors and Actuators A: Physical*, vol. 116 issue 3 p. 450 https://doi.org/10.1016/j.sna.2004.05.014

[35] Z. G. Zhou, – Z. L. Tang – Z. T. Zhang (2005) mpedance Analysis Study on the Sensing Process of BaTiO3 Based PTC Ceramics in CO Gas, Key Engineering Materials vol. 280 p. 369 https://doi.org/10.4028/www.scientific.net/KEM.280-283.369

[36] A. Jamaluddin et al (2016) Properties of strontium doped barium titanate powder prepared by solid state reaction, J. Phys.: Conf. Ser. Vol. 776 012052 https://doi.org/10.1088/1742-6596/776/1/012052

[37] W.J. Dawson 1988 *American Ceramic Society Bulletin*, vol. 67 no. 10 p. 1673

[38] S. Komarneni, I. R. Abothu Et A. V. P. Rao (1999) Sol-Gel Processing of Some Electroceramic Powders, J. Sol-Gel Sci. Techno. Vol. 15 p 263 https://doi.org/10.1023/A:1008793126735

[39] G.R. Fox, J.H. Adair and R.E. Newnham (1990) Effects of pH and H2O2 upon coprecipitated PbTiO3 powders, *Journal of Materials Science* vol. 25 issue 8 p. 3634 https://doi.org/10.1007/BF00575398

[40] A. Mahapatra, S. Parida, S. Sarangi and T. Badapanda (2015) Dielectric and Ferroelectric Behavior of Bismuth-Doped Barium Titanate Ceramic Prepared by Microwave Sintering, *JOM* vol. 67 issue 8 p. 1896 https://doi.org/10.1007/s11837-014-1266-7

[41] A. Rani, J. Kolte, S.S. Vadla and P. Gopalan (2016) Structural, electrical, magnetic and magnetoelectric properties of Co-doped BaTiO3 multiferroic ceramics, *Ceramics International*, vol. 44 issue 14 p. 16703 https://doi.org/10.1016/j.ceramint.2018.06.098

[42] P.P. Khirade, S.D Birajdar, A.V. Raut and K.M. Jadhav (2016) Effect of Fe – substitution on phase transformation, optical, electrical and dielectrical properties of BaTiO3 nanoceramics synthesized by sol-gel auto combustion method, *Journal of Electroceramics* vol. 37 issue 1-4 p. 110 https://doi.org/10.1007/s10832-016-0044-z

[43] N. Maikhuri, A.K. Panwar and A.K. Jha (2013) Investigation of A- and B-site Fe substituted BaTiO3 ceramics, Journal of Applied Physics vol. 113 17D915 https://doi.org/10.1063/1.4796193

[44] U. Holzwarth and N. Gibson (2011) The Scherrer equation versus the ‚Debye-Scherrer equation', Nature Nanotechnology vol. 6 no. 9 p. 534 https://doi.org/10.1038/nnano.2011.145

[45] G.K. Williamson and W.H. Hall (1953) X-ray line broadening from filed aluminium and wolfram, Acta metallurgica vol. 1 issue 1 p. 22 https://doi.org/10.1016/0001-6160(53)90006-6

[46] X. Jin, D. Sun, M. Zhang, Y. Zhu and J. Qian (2009) Investigation on FTIR spectra of barium calcium titanate ceramics, *Journal of electroceramics* vol. 22 issue 1-3 p. 285 https://doi.org/10.1007/s10832-007-9402-1

[47] R. Ashiri, A. Nemati, M.S Ghamsari, S. Sanjabi and M. Aalipour (2011) A modified method for barium titanate nanoparticles synthesis, *Materials Research Bulletin* vol. 46 issue 12 p. 2291 https://doi.org/10.1016/j.materresbull.2011.08.055

Ref.:
Tihtih, Mohammed – **Limame,** Karoum – **Ababou,** Yahya – **Sayouri,** Salaheddine – **Ibrahim,** Jamal-Eldin F. M.: *Sol-gel synthesis and structural characterization of Fe doped barium titanate nanoceramics*
Építőanyag – Journal of Silicate Based and Composite Materials, Vol. 71, No. 6 (2019), 190–193. p.
https://doi.org/10.14382/epitoanyag-jsbcm.2019.33

Effect of H_2 on SiO and SiC formation

Trygve Storm AARNÆS
Is PhD candidate in the Norwegian University of Science and Technology (NTNU) at Department of Materials Science and Engineering, Norway.

Merete TANGSTAD
Since 2004 she has been a professor at Department of Materials Science and Engineering in NTNU, Norway and her main fields are ferralloy production, silicon production and solar grade silicon processes.

Trygve Storm AARNÆS ▪ Department of Materials Science and Engineering, Norwegian University of Science and Technology, Norway ▪ trygve.s.aamas@ntnu.no
Merete TANGSTAD ▪ Department of Materials Science and Engineering, Norwegian University of Science and Technology, Norway ▪ merete.tangstad@ntnu.no

Érkezett: 2019. 11. 29. ▪ Received: 29. 11. 2019. ▪ https://doi.org/10.14382/epitoanyag-jsbcm.2019.34

Abstract

Based on previous research, hydrogen has an enhancing effect on the kinetics of the Si-O-C system [1-3]. In this study silicon carbide (SiC) formation, from a reaction between SiO(g) and carbon, were investigated in a hydrogen atmosphere, an argon atmosphere, and an argon atmosphere containing 10% methane, at temperatures between 1495 °C and 1695 °C. The SiO(g) was generated from pellets comprised of a 2:1 ratio of silica (SiO_2) and SiC. The SiO(g) generation was monitored through analysis of the CO(g) content of the off-gas, the results indicated that the hydrogen atmosphere had an enhancing effect on SiO(g) generation through this reaction. Samples were retrieved from various locations within the set-up: the crucible, the reaction chamber roof, and from the condensation chamber. The reaction products were imaged in SEM using secondary electrons.

SiC was found growing throughout the reaction chamber, when using an argon atmosphere, a layer of SiC was found covering the graphite parts, whereas utilising a hydrogen atmosphere, or argon with 10% methane, the SiC would instead grow as whiskers. Thermal decomposition of methane is expected to be a challenge in this temperature range [4].

Keywords: silicon, SiC, hydrogen, methane, whiskers
Kulcsszavak: szilícium, SiC, hidrogén, metán, whisker

1. Introduction

Silicon is currently produced in a submerged arc furnace from a reaction between SiO_2 and carbon. SiO_2 is supplied from high purity quartz, and commonly used carbon sources include: wood chips, charcoal or coal [5]. One of the most important intermediate species occurring during silicon production is SiO(g). It is formed in the hot lower region of the furnace from a reaction between SiO_2 and silicon carbide (SiC), reaction (1), and is consumed in the cooler upper region where it reacts with the carbon in the charge to form SiC, reaction (2). When SiO(g) is cooled down it will form Si and SiO_2 according to reaction (3), it may also form SiO_2 and SiC according to reaction (4). These reactions are commonly called the condensation reactions [5-6].

$$2\,SiO_2 + SiC = 3\,SiO(g) + CO(g)\quad SiO(g) + 2\,C = SiC + CO(g) \quad (1)$$
$$2\,SiO(g) = 2\,SiO_2 + Si\quad 2SiO(g) + 2\,CO(g) = SiO_2 + SiC \quad (2)$$
$$2\,SiO(g) = 2\,SiO_2 + Si \quad (3)$$
$$2\,SiO(g) + 2\,CO(g) = SiO_2 + SiC \quad (4)$$

Producing silicon consumes large amounts of energy. It is supplied, in part, from electricity, and in part from solid carbon materials. Finding a replacement to the carbon materials could lead to significant reductions in CO_2 emissions. Thus far there has been some research into possible alternatives to carbon for reducing metal oxides [7-9]. Most of the work has been on the use of methane hydrogen mixtures [10-11]. Despite the fact that CH_4(g) contains carbon, which will lead to CO_2(g) emissions, it may allow a more efficient process to be designed, or if bio-gas was utilised the net-CO_2(g) emissions would also be lowered. While some metals, such as iron, may be readily reduced to its metallic form by hydrogen, silicon has a much stronger affinity to oxygen making the reduction process more challenging [9]. One of the key challenges that face the use of CH_4(g) in silicon production is that the gas is unstable at high temperatures, and will undergo thermal cracking to H_2(g) and carbon according to reaction [4]. According to its thermodynamic equilibrium, CH_4(g) will be almost completely transformed to carbon and H_2(g). However, literature reports that methane cracking often occurs far away from its thermodynamic equilibrium if it does not happen on a suitable catalyst [12]. Furthermore, the deposited carbon is a poor catalyst for this reaction, so as CH_4(g) cracks it will form a layer which limits further cracking [4], [13]. Similarly, SiO(g) will form a condensate at low temperatures. Thus, there is a large temperature gap between the regions where each of the gasses are stable. Therefore, it is important to research how far away from their respective equilibrium pressures it is possible to go.

$$CH_4(g) = C + 2\,H_2(g) \quad (5)$$

This study aims to investigate the reaction between SiO(g) and carbon, and how it is influenced by different hydrogen containing atmospheres. In addition, the extent of thermal cracking of CH_4(g) will be examined, and whether it is possible to have CH_4(g) and SiO(g) react.

2. Experimental

SiO(g) and CO(g) were produced from pellets made from pure quartz and pure SiC which was crushed to a size of 5 mm. The quartz and SiC was pelletized and mixed with a molar ratio of 2:1, which follows the stoichiometry of reaction (1). A

schematic drawing of the set-up is shown in *Fig. 1*. It consists of two main parts: a reaction chamber which is the bottom section, and a condensation chamber which is the top section. The reaction chamber contained a graphite crucible, which was filled with approximately 5 g of pellets before each experiment. An alumina lance was inserted into the reaction chamber from the top of the set-up. The condensation chamber consisted of a graphite tube surrounded by graphite wool insulation. While preparing the experiment, the alumina tube was placed through the middle of the condensation chamber in such a way that it protruded 2.5 cm into the reaction chamber. Additionally, a C-type thermocouple was passed through the lance so that its tip was in the center of the reaction chamber. After inserting the lance, SiC particles were poured into the space between the lance and the condensation chamber wall, which were added to collect reaction products.

After the set-up had been prepared according the description in the previous paragraphs, it was placed into the furnace. The furnace was a resistance heated vertical tube furnace. The off-gas from the furnace went through a gas analyser which detected the CO(g) content. First, the furnace was flushed with argon and evacuated down to 180 mbar, then it was refilled with argon as the temperature program commenced.

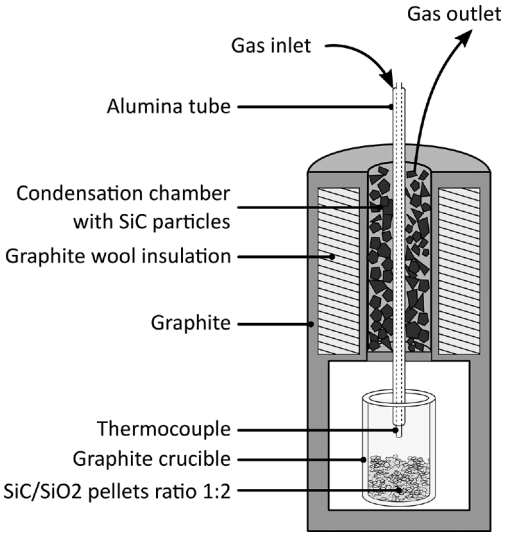

Fig. 1 Set-up used to investigate the reaction between the SiO(g) and CO(g), and carbon in an Ar(g) and an H_2(g) atmosphere
1. ábra A SiO(g) és CO(g), valamint a szén reakciója Ar(g) és H_2(g) atmoszférában

The temperature measured within the reaction chamber was observed to be lower than the furnace set-point, which was 1750°C, 1650°C or 1550°C. *Fig. 1* shows the temperature measurements from the reaction chamber. It shows that the real temperature in the reaction chamber is around 55°C lower than the set-point of the furnace, the thermocouple is measuring the temperature in the centre of the reaction chamber. The parameters which were varied between experimental runs were the holding temperature, which was either 1595°C, 1695°C, or 1495°C and the process gas mixture which was a H_2(g)/CH_4(g) gas mix that was varied between 0% CH_4(g) and 10% CH_4(g). The experimental matrix displayed in *Table 1* shows the number of experiments performed for each combination of parameters. After each experiment, samples were taken from various regions of the set-up. They were taken from the crucible rim, the ceiling of the reaction chamber, the graphite ring on the bottom of the condensation chamber, the alumina lance, and SiC chunks in the condensation chamber. The samples were placed into a SEM and imaged with a secondary electron detector.

		Methane content in a CH4(g)/ Ar gas mix	
	Pure H_2(g)	0%	10%
1695°C	2	1	0
1595°C	2	1	1
1495°C	0	1	0

Table 1 Experimental matrix, the number in each cell indicates number of parallels
1. táblázat Kísérleti mátrix, az egyes cellákban szereplő számok a párhuzamok számát jelzik

3. Results/Discussion

3.1 Generation of SiO(g) from the raw material

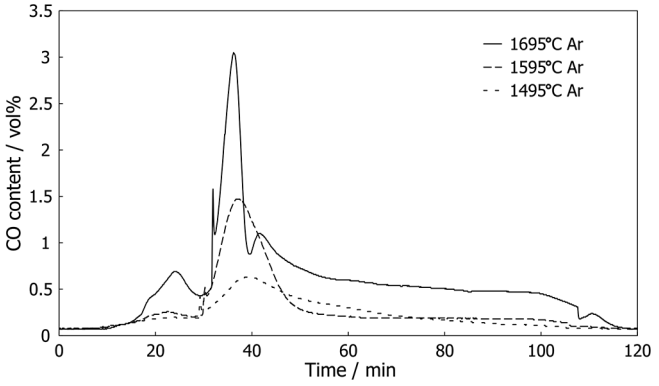

Fig. 2 CO(g) content of the off-gas for experiments in an Ar atmosphere at various temperatures
2. ábra A kiáramló gáz CO(g)-tartalmának vizsgálata Ar atmoszférában, különböző hőmérsékleteken

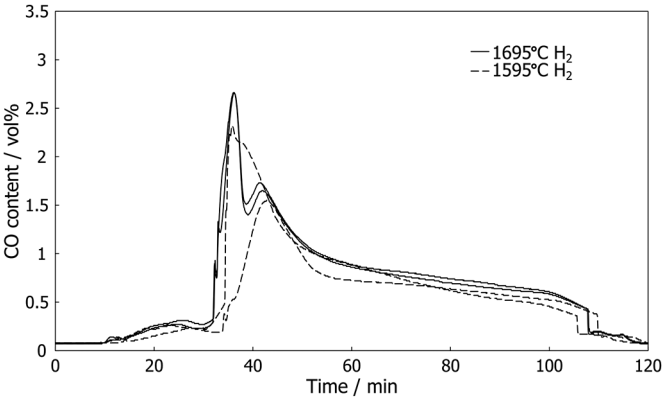

Fig. 3 CO(g) content of the off-gas for experiments in an H_2(g) atmosphere at various temperatures
3. ábra A kiáramló gáz CO(g)-tartalmának vizsgálata H_2(g) atmoszférában, különböző hőmérsékleteken

Isothermal experiments in an argon/CH_4(g)/H_2(g) atmosphere were performed. The reaction was monitored through measurement of the CO content of the off-gas. *Fig. 2* shows the off-gas measurements for the experiments in an

argon atmosphere at 1495°C, 1595°C and 1695°C. *Fig. 3* shows the off-gas measurements for the experiments in a $H_2(g)$ atmosphere at 1595°C and 1695°C.

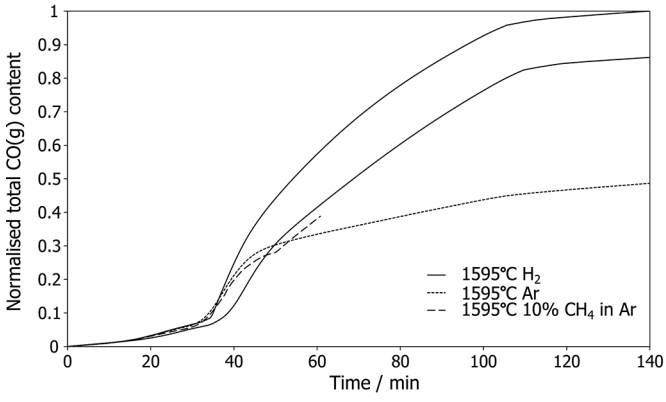

Fig. 4 Normalised integral CO(g) formation during experiments in pure $H_2(g)$, Ar(g) and Ar with 10% $CH_4(g)$, at 1595°C
4. ábra Normál integrált CO(g) képződés vizsgálata tiszta $H_2(g)$, Ar(g) és Ar 10% $CH_4(g)$ összetételű atmoszférában 1595°C-on

Fig. 4 shows a comparison of the normalised integral CO(g) content of the off-gas, with $H_2(g)$, Ar, and Ar with 10% $CH_4(g)$, at 1595°C. The most obvious trend of the off-gas CO(g) content is that it increases with temperature, at least in an Ar(g) atmosphere. Which is an indication of the raw material being converted to SiO(g) and CO(g) at a more rapid pace. However, when the atmosphere is exchanged with pure $H_2(g)$, the effect of temperature is not so obvious. Furthermore, after the initial peak in the CO(g) content, the curves follow each other closely for the rest of the temperature program. Thus, as a result of using an $H_2(g)$ atmosphere, the SiO(g) content in the reaction chamber is increased.

The weight of the pellets which were recorded before and after each experiment are consistent with what was seen in the CO(g) content of the off gas. *Table 2* shows what weight change was seen at different temperatures and atmospheres, evident that much more of the pellets were transformed to SiO(g) in an $H_2(g)$ atmosphere than in Ar(g).

Temperature	Mass change in Ar(g)	Mass change in $H_2(g)$
1695 °C	.	-57.9%
1595 °C	-14.4%	-45.7%
1495 °C	-12.4%	-

Table 2 Mass change of the raw material for each experiment
2. táblázat A nyersanyag tömegváltozása a kísérleteknél

3.2 Formation of SiC

SiC crystals could be seen growing in the rim of the graphite crucible. At the cooler temperature, the crystals are much smaller and large ones are more sparsely distributed on the surface. In an $H_2(g)$, or Ar(g) with 10% $CH_4(g)$ atmosphere the surface of the crucible is covered in SiC whiskers. Growth of SiC whiskers in $H_2(g)$ containing atmospheres has been seen previously. The most common explanation for growth of SiC in $H_2(g)$ containing atmospheres is that presence of hydrogen allows $CH_4(g)$ to form in small quantities. This would allow for an enhanced gas phase transfer of carbon which is necessary to grow long SiC whiskers [1], [14]. Improved diffusion in $H_2(g)$ may also contribute. Reaction (6) and (7) show how $CH_4(g)$ might provide a means for gas phase carbon transfer to the whisker tips.

$$C + 2\ H_2(g) = CH_4(g) \quad (6)$$

$$SiO(g) + CH_4(g) = SiC(s) + CO + 2\ H_2(g) \quad (7)$$

In Si containing systems the growth mechanisms of whiskers most often cited are vapour-liquid-solid (VLS), where there is a liquid impurity that acts as a catalyst to the whisker growth, vapour-solid (VS) where there is no catalyst, and oxide assisted growth (OAG) where there is layer of molten SiO_2 around the tip [15]. However, regardless of which of these growth mechanisms are present in this work, all of them require gas phase transfer of carbon from the graphite parts to the whisker tip. The two options are through $CO(g)/CO_2(g)$ or $H_2(g)/CH_4(g)$. Considering that the equilibrium $CH_4(g)$ pressure is larger by a factor of 1000, compared to $CO_2(g)$, in this temperature range $H_2(g)/CH_4(g)$ is expected to play a bigger role [16-17].

4. Conclusions

The $H_2(g)$ atmosphere had an enhancing effect on the SiO(g) formation in the raw materials. Additionally. the SiO(g) formation in an $H_2(g)$ atmosphere was much less affected by temperature than in a pure Ar(g) atmosphere.

SiC formation in the current experimental set-up was enhanced in an $H_2(g)$ atmosphere compared to an Ar(g) atmosphere. There are a few possible explanations, the presence of $H_2(g)$ allowed for a kinetically more favoured reaction path to SiC formation. The increased SiO(g) formation leads to a higher SiO(g) content throughout the reaction chamber which would increase SiC formation. Faster diffusion in the $H_2(g)$ atmosphere may also play a role in the improved kinetics. Furthermore, the SiC formed in an $H_2(g)$ atmosphere grew as whiskers, while in an Ar(g) atmosphere it grew as a layer covering the graphite. The difference is suspected to be caused by the formation of $CH_4(g)$ from the $H_2(g)$ reacting carbon, and the $CH_4(g)$ allows for fast gas phase carbon transfer to the whisker tip.

References

[1] Li, X. – Zhang, G. – Tronstad, R. – Ostrovski, O. (2016): Synthesis of SiC whiskers by VLS and VS process, *Ceramics International,* vol. 42, no. 5, pp. 5668-5676
[2] Bootsma, G. A. – Knippenberg, W. F. – Verspui, G. (1971): Growth of SiC whiskers in the system SiO_2-C-H_2 nucleated by iron, *Journal of Crystal Growth,* vol. 11, no. 3, pp. 297-309
[3] Ksiazek, M. – Tangstad, M. – Dalaker, H. – Ringdalen, E. (2014): Reduction of SiO_2 to SiC Using Natural Gas, *Metallurgical and Materials Transactions E,* vol. 1, no. 3, pp. 272279
[4] Amin, A. M. – Croiset, E. – Epling, W. (2011): Review of methane catalytic cracking for hydrogen production, *International Journal of Hydrogen Energy,* vol. 36, no. 4, pp. 2904-2935
[5] Tangstad, M. (2013): *Metal production in Norway.* Oslo: Akademika Publ
[6] Schei, A. (1998): *Production of high silicon alloys.* Trondheim: Tapir
[7] Ostrovski, O. – Zhang, G. (2006): Reduction and carburization of metal

oxides by methane- containing gas, *AIChE Journal,* vol. 52, no. 1, pp. 300-310
[8] Kononov, R. – Ostrovski, O.– Ganguly, S. (2008): Carbothermal Reduction of Manganese Oxide in Different Gas Atmospheres, *Metallurgical and Materials Transactions B,* vol. 39, no. 5, pp. 662-668
[9] Ostrovski, O. – Zhang, G. – Kononov, R. – Dewan, M. A. R. – Li, J. (2010): Carbothermal Solid State Reduction of Stable Metal Oxides, *steel research international,* vol. 81, no. 10, pp. 841-846
[10] Ebrahim, H. Ale – Jamshidi, E. (2005): Kinetic Study and Mathematical Modeling of the Reduction of ZnO-PbO Mixtures by Methane, *Industrial & Engineering Chemistry Research,* vol. 44, no. 3, pp. 495-504
[11] Zhang, G. – Ostrovski, O. (2000): Reduction of titania by methane-hydrogen-argon gas mixture, *Metallurgical and Materials Transactions B,* vol. 31, no. 1, pp. 129-139
[12] Holmen, A.– Olsvik, O. – Rokstad, O. A. (1995): Pyrolysis of natural gas: chemistry and process concepts, *Fuel Processing Technology,* vol. 42, no. 2-3, pp. 249-267
[13] Alizadeh, R. – Jamshidi, E. – Zhang, G. (2009): Transformation of methane to synthesis gas over metal oxides without using catalyst, *Journal of Natural Gas Chemistry,* vol. 18, no. 2, pp. 124-130
[14] Li, X. – Zhang, G. – Ostrovski, O. – Tronstad, R. (2016): Effect of gas atmosphere on the formation of silicon by reaction of SiC and SiO_2, *Journal of Materials Science,* vol. 51, no. 2, pp. 876-884
[15] S. Noor Mohammad (2009): For nanowire growth, vapor-solid-solid (vapor-solid) mechanism is actually vapor-quasisolid-solid (vapor-quasiliquid-solid) mechanism, *The Journal of Chemical Physics,* vol. 131, no. 22, p. 224702
[16] *HSC9.* Outotec (2019)
[17] Yew, K. – Ling, Y. (2010): Advances of SiOx and Si/SiOx Core-Shell Nanowires, in *Nanowires Science and Technology,* N. Lupu, Ed. InTech

Ref.:
Aarnæs, Trygve Storm – **Tangstad,** Merete: *Effect of H_2 on SiO and SiC formation*
Építőanyag – Journal of Silicate Based and Composite Materials, Vol. 71, No. 6 (2019), 194–197. p.
https://doi.org/10.14382/epitoanyag-jsbcm.2019.34

Thermal stability and flame retardant properties of plasticized poly(vinyl chloride) hybrid composite for construction application

Ali I. AL-MOSAWI ▪ Institute of Ceramic and Polymer Engineering, University of Miskolc, Hungary ▪ aliibrahim76@yahoo.com

Kálmán MAROSSY ▪ Institute of Ceramic and Polymer Engineering, University of Miskolc, Hungary ▪ qkoali76@uni-miskolc.hu

Érkezett: 2019. 11. 29. ▪ Received: 29. 11. 2019. ▪ https://doi.org/10.14382/epitoanyag-jsbcm.2019.35

Abstract

Current research is investigating how to improve constructions efficiency and at the same time increase their fire resistance. Oxydtron is used as admixture for concrete to improve its properties, but Oxydtron has shown unpredictable behavior when used as filler for plasticised PVC where the flame retardation and stabilization at high temperatures of the polymer was improved after Oxydtron additions. Thermal tests were carried out to demonstrate the ability of Oxydtron to improve thermal resistance of the plasticised PVC and these tests included: Limiting oxygen index, Dehydrochlorination, and Dynamic mechanical analysis. The results of these tests proved the efficiency of Oxydtron as effective filler for plasticised PVC by increasing the flame retardation and thermal stability.

Keywords: thermal stabilizing, flammability, oxydtron, plasticized poly(vinyl chloride)
Kulcsszavak: hőstabilitás, éghetőség, oxydtron, lágyított PVC

Ali I. AL-MOSAWI
PhD student in Polymers engineering Institute of Ceramic and Polymer Engineering, Faculty of Material Science and Engineering, University of Miskolc, Hungary. M.Sc. and B.Sc. Materials Engineering, Faculty of Engineering, University of Babylon, IRAQ. Research interests: Polymers, Composite materials, Rubber technology, Flame retardants, Material testing, Materials processing.

Kálmán MAROSSY
Professor of Polymers engineering at Institute of Ceramic and Polymer Engineering, University of Miskolc, Hungary. Recent research interests: Polymer blends, Multiphase polymer systems, Relaxation phenomenon, Polymer degradation, Composite materials, Rubber.

1. Introduction

When Prometheus stolen the fire from the Hephaestus god of blacksmiths in Mount Olympus according to the Greek mythology and gave it to humans to help them overcome the difficulties of their daily lives related to heating, lighting and cooking; he didn't realize that fire would be useful to humans but also would bring destruction to them if they didn't use it safely. So, they have tried to find the methods to extinguish fire. Then they thought of something entirely new: creating materials that could resist fires reduce their risk and even completely stop it, thus, the concept of flame retreading appeared for the first time; and the subsequent discovery of materials (flame retardants) have the ability to break the cycle of fire [1,2]. As the concept of flame retardation developed, it was necessary to develop the way of thinking in this field; now, the search for new and unconventional materials in industry is imperative to balance environmental considerations for the safe use of non-polluting materials (or at least with limited damage) and to maintain the best possible achievement of new materials compared to traditional materials. Where the purpose is not only to use new engineering materials in the industry, but to be more efficient or at least maintain the same level of performance of the traditional materials currently available which can be termed metaphorically - the sustainability of properties - as with the sustainability of natural materials, otherwise there will be no benefit from Use of such materials [3-6]. Every year, fires cause a significant human and financial losses in all countries, and the proportion of these losses varies from one country to another depending on the equipment and techniques used to reduce the fires risk, as shown in *Table 1* and *Fig. 1*, which are represented the economic-statistical evaluation of fire costs according to the center of fire statistics report issued in the year 2016 [7]. As shown in *Table 1*. Many countries still don't attach much importance to fire protection, but spend much of their gross domestic product (GDP) to extinguish the fires after ignite, but it is best to be concerned with how to prevent the fire from happening.

In general, the principle of reducing fire rates depends on the provision of conventional fire extinguishing equipment; use of materials with low flammability ranges or improve their thermal resistance if they are highly flammable such as polymers; appropriate design of the buildings to provide outlets to escape when the fire to reduce the loss of human, and all the above points are relevant to the important factor which is the deployment of a "fire prevention culture" that is fully dependent on people's awareness of fire hazards and the extent to which they apply safety arrangements to prevent fires or reduce it [8,9]. Poly(vinyl chloride) is one of the most important types of polymers used today in the plastics industry and has maintained its position in this industry despite its long discovery and the emergence of many new polymers due to its distinctive properties. Poly(vinyl chloride) can be produced in more than one state, which is rigid and flexible. The important thing is that changing poly(vinyl chloride) from rigid to flexible state there's no need to change its chemical formula through polymerization but through additives only, which is not available in the majority of other polymers. These additives improve many of the polymers properties in general, and one of these properties is thermal resistance, where all polymers not just poly(vinyl chloride) have low thermal resistance to high temperatures which considered an obstacle to the use of such materials in applications requiring high thermal resistance. Therefore, there is a high risk of using them in civil and industrial applications without increasing their resistance to combustion [3,10-20].

N	Country	Cost in portion of GDP, %					$\sum_{i=1}^{5} C_i$	Expenditure / losses $\frac{C3+C4+C5}{C1+C2}$
		Direct losses C_1	Indirect losses C_2	Cost of fire service C_3	Fire protection in buildings C_4	Fire insurance administrations C_5		
1	Australia	0.07	-	0.17	-	-	-	-
2	Czech Republic	0.07	-	-	0.16	-	-	-
3	Finland	0.17	0.011	0.19	-	0.03	-	-
4	France	0.20	-	-	-	-	-	-
5	Germany	0.12	0.014	-	-	-	-	-
6	Hungary	0.02	-	0.13	-	-	-	-
7	Italy	0.02	-	-	0.35	0.04	-	-
8	Japan	0.12	0.060	0.26	0.12	0.09	0.650	2.61
9	Netherlands	0.15	-	0.21	0.31	-	-	-
10	New Zealand	0.12	-	0.16	0.24	-	-	-
11	Poland	0.09	-	0.16	-	-	-	-
12	Singapore	0.04	0.027	0.03	0.40	0.02	0.517	6.72
13	Spain	0.08	-	-	-	-	-	-
14	Sweden	0.18	0.060	0.13	0.20	0.05	0.620	1.58
15	UK	0.13	0.008	0.20	0.29	0.10	0.728	3.84
16	USA	0.10	0.007	0.29	0.29	0.12	0.807	6.54
	Avrg.	**0.12**	**0.027**	**0.18**	**0.26**	**0.05**	**0.652**	**3.40**

Table 1 Economic-statistical evaluation of fire costs [7]
1. táblázat Tűzesetek költségeinek gazdasági elemzése [7]

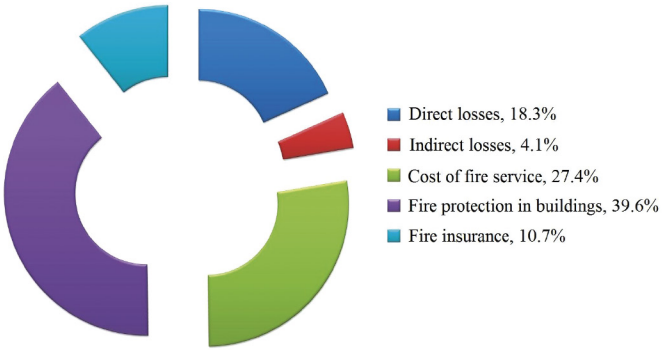

Fig. 1 Economic-statistical evaluation graph of fire costs [7]
1. ábra A tűzesetek költségeinek gazdasági elemzése [7]

Oxydtron one of the non-traditional additive that we used in this study. Those who hear about Oxydtron for the first time are thought to contain nanoparticles as indicated by the name but this is not true where the cement is a micro particles powder (about 2-3 μm) and just the particle's coating layer which consists of modifier materials is nano size (from 10-100 nm); which gives this material special characteristics in addition to its low cost. Oxydtron contains many of the high-temperature oxides and carbonates that make it one of the most important and alternative options for conventional retardants used today [21-23].

2. Methodology

2.1 Materials

The raw materials used for producing tests samples illustrated in *Table 2* which can be described as follows: (1) PVC S-5070 powder (under trademark Ongrovil®) which produced and supplied by BorsodChem Zrt., Hungary; (2) the plasticizer DOP (Di-Octyl Phthalate) supplied by DEZA, a. s. CO., Valašské Meziříčí, Czech Republic; (3) Calcium-Zinc based stabilizer (under trademark Newstab-50) which supplied by Betaquímica CO., Barcelona, Spain; (4) the lubricant Wax-E (under trademark Licowax®E) supplied by Clariant International Ltd, Muttenz Switzerland; and (5) Oxydtron (NC) (under trademark Oxydtron-Oxydtron type A) supplied by Bioekotech Hungary Kft.

Component	PVC basic formulation				PVC modifier
	PVC S-5070	DOP	Newstab-50	Wax-E	Oxydtron
pphr	100	70	1.5	0.3	0-5 (wt.%)

Table 2 Raw materials for producing test samples and their dosage
2. táblázat Próbatestek készítéséhez használt alapanyagok és adagolásuk

2.2 Materials processing

The main mixing process involved mixing all the raw materials listed in *Table 2*, which accomplished using a mechanical mixer type MTI 10 Mischtechnik at 150 °C; in order to obtain homogeneity in the mixture. After the main mixing process, the Oxydtron is added with the weight fraction (0, 1, 3, and 5) wt.%. The new hybrid blend has been mixed by small electric mixer to provide homogeneous distribution of Oxydtron within the poly(vinyl chloride) powder.

2.3 Samples fabrication

1. Limiting oxygen index samples: L.O.I samples were produced according to ISO 4589-2 standard [24] by using also laboratory two roll mill type Schwabenthan at the same processing conditions. A sheets with 0.4 -0.6 mm thickness made by rolling and then these sheets compressed by a hydraulic press type Bürkle at 300 and 20 bar pressure and 175 °C to the desired L.O.I sample shape.

2. Dehydrochlorination test: a particle of PVC and Oxydtron additives with the same dimensions of congo-red test was used in this test at 170 °C and according to ISO 182-3:1993 standard [25].
3. Dynamic mechanical analysis test: ISO 6721-11:2012 standard [26] was used to produce the samples. The DMA test samples were a strips fabricated by using extrusion machine type GÖTTFERT at 170 °C temperature and 60 rpm speed at uniform conditions (pressure, temperature, and compression).

2.4 The tests

1. Limiting oxygen index test: This test was done at BorsodChem Zrt., Laboratory of Vinyl Technology by using Stanton Redcroft FTA flammability unit.
2. Dehydrochlorination test: Dehydrochlorination ranges have been measured by Metrohm 763 Thermomat device found also at BorsodChem Zrt., Hungary.
3. Dynamic mechanical analysis test: Dynamic mechanical thermal analyser MK III manufactured by Rheometric Scientific, Inc. and found at BorsodChem Zrt., Hungary, used for testing the samples. The temperature range is -60 °C to 120 °C.
4. Scanning electron microscopy (SEM): In order to analyse the elemental composition and structure of Oxydtron, the Carl Zeiss EVO MA10 SEM was used for performed this analysis as shown in *Fig. 2* and *Table 3*. SEM device found at Institute of Physical Metallurgy, Metal Forming and Nanotechnology, University of Miskolc, Hungary.
5. Oxides analysis: ICP-AES spectrometer was used for the analysis of Oxydtron components. The results of the analysis are listed in *Table 4*. ICP-AES spectrometer found at Institute of Chemistry, University of Miskolc, Hungary.

Element	Wt.%	At %	Net Inte.	Bkgd Inte.	Inte. Error	P/B
C	7.57	14.33	22.07	1.00	4.06	22.07
O	34.78	49.43	121.40	1.50	1.68	80.93
Na	0.64	0.63	6.53	3.87	10.56	1.69
Mg	0.77	0.72	11.23	5.73	7.74	1.96
Al	2.09	1.76	36.63	7.03	3.55	5.21
Si	10.45	8.46	195.23	9.40	1.37	20.77
S	1.48	1.05	27.37	9.90	4.58	2.76
K	1.08	0.63	18.13	8.00	5.88	2.27
Ca	38.85	22.04	563.83	7.70	0.78	73.23
Ti	0.17	0.08	1.70	6.00	39.75	0.28
Fe	2.12	0.86	12.63	3.67	6.46	3.45

Table 3 EDAX- SEM analyses for structural composition of Oxydtron
3. táblázat Az Oxydtron összetételének SEM – EDAX analízise

Oxides	Ratio, wt.%
Al_2O_3	4.47
CaO	58.0
Cr_2O_3	0.006
Fe_2O_3	2.67
K_2O	0.78
MgO	1.20
Mn_2O_3	0.05
Na_2O	0.31
SO_3	2.50
SiO_2	21.44
TiO_2	0.274
ZnO	0.138

Table 4 Chemical composition of Oxydtron analyzed by ICP-AES
4. táblázat Az Oxidtron kémiai összetételének meghatározása ICP-AES módszerrel

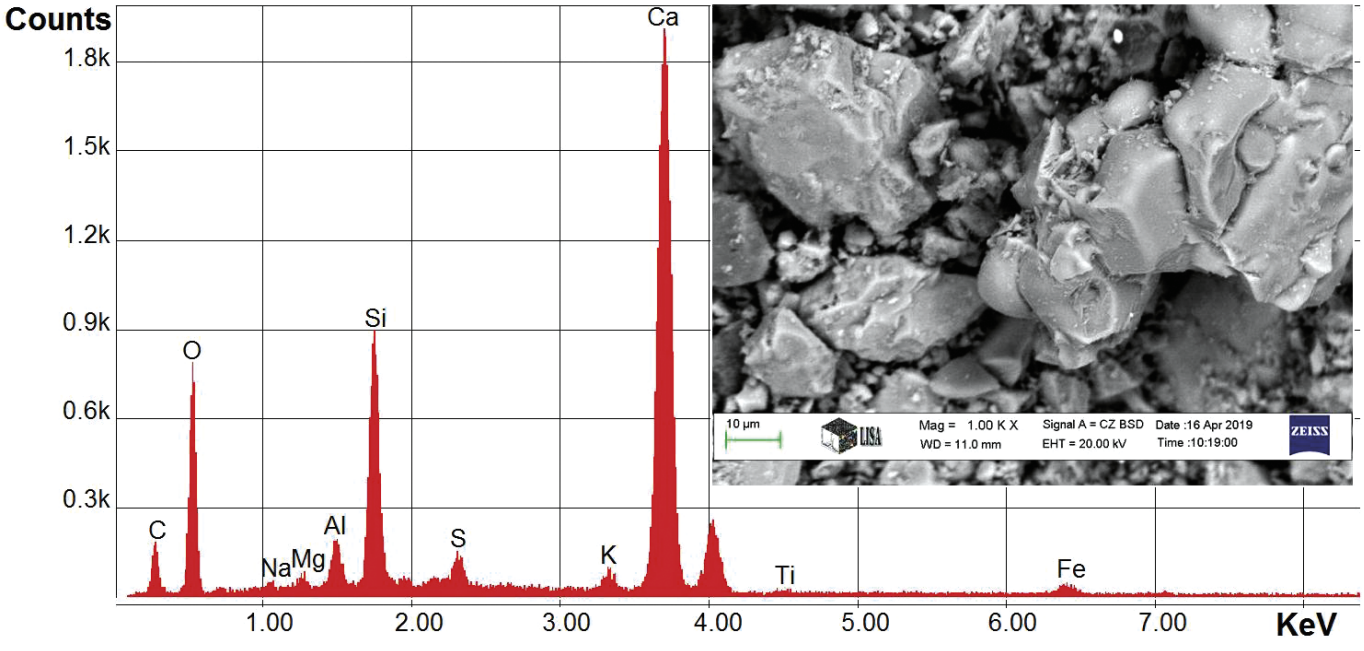

Fig. 2 SEM-energy dispersive X-ray microanalysis for Oxydtron
2. ábra Az Oxydtron SEM energiadiszperzív Röntgen mikroanalízise

4. Results and descussion

Flame retarding results for plasticised PVC containing Oxydtron obtained by limiting oxygen index (L.O.I) test shown in *Fig 3.* From the first bar of this figure which represents the L.O.I. result of plasticised PVC basic formulation that the value of L.O.I is low (21.6%). The low flame resistance considered a normal state for plastics and this low resistance because of the crystalline structure of these materials (especially organic) therefore it will ignite easily and rapidly when exposed to direct fire [1,3]. And in order to modify this critical behavior of plastics at high temperatures (PVC in this study), the additives are added to increase their thermal resistance. These additives can be used as fillers or coating layers [27,28]. After adding 1% Oxydtron as a new flame retardant additive for plasticised PVC fire resistance of the polymer improves as shown in the second bar of *Fig. 3* where the L.O.I value has been increased to (22.3%). The flame resistance of plasticised PVC is increasingly rising with increasing Oxydtron additives quantity which can be observed in the third bar of *Fig. 3* which represents the L.O.I value of plasticised PVC containing 3% Oxydtron where the L.O.I value reached to (24.8%), while it will reach a value of (26.4%) as shown in the fourth bar which represents L.O.I value of plasticised PVC containing 5% Oxydtron. This unexpected behavior of Oxydtron stabilizing and flame retarding is due to Oxydtron composition which consists of many compounds such as calcium carbonate ($CaCO_3$) which considered a universal stabilizer for PVC and also silicon dioxide (SiO_2) in addition to many other compounds, and these two materials ($CaCO_3$ and SiO_2) will act as a synergist agent with the Newstab-50 (original stabilizer) and creating additional stabilizing synergistic action causing increased thermal resistance and stability of plasticised PVC. Also, the calcium carbonate considered a flame retardant agent and its presence within the Oxydtron composition will help to increase the flame resistance of PVC.

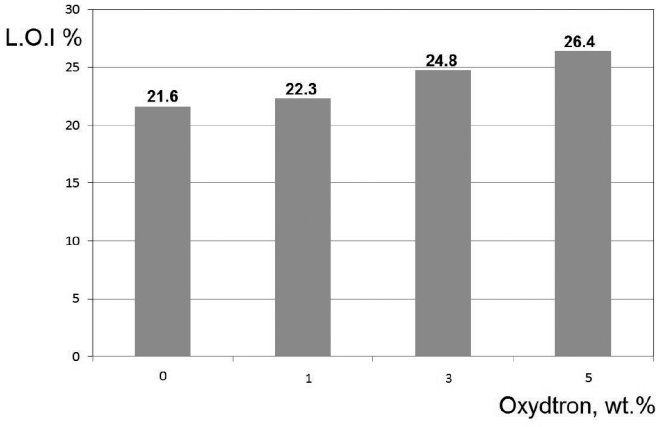

Fig. 3 Limiting oxygen index (L.O.I) values for plasticised PVC-Oxydtron hybrid composite
3. ábra Az Oxidtron tartalmú lágy PVC keverékek oxygen indexe (LOI)

The crystalline structure of PVC tends to release chlorine containing compounds strongly at high temperatures, as shown in *Fig. 4*, which represents a dehydrochlorination test for plasticised PVC basic formulation at 170 °C; where the chlorine containing compounds loss is very rapid and the slope of the curve is very sharp (high inclination). This is a normal behaviour for PVC due to the low thermal resistance in high temperatures (for polymers) and this resistance decreases as the release of chlorine containing compounds increases where the crystalline structure of PVC is strongly deformed; and the bonds between atoms begin to break down and huge amounts of chlorine containing compounds are released [29]. This is observed from the high slope of the curve (0.000134) and at this point, the PVC reached the degree of total degradation.

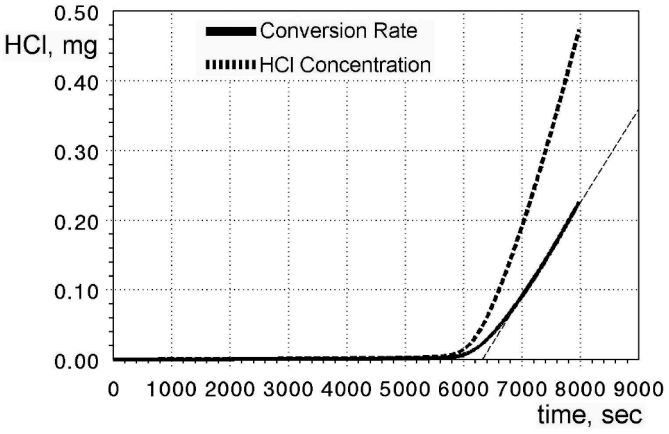

Fig. 4 Dehydrochlorination test of plasticised PVC basic formulation at 170 °C
4. ábra A PVC alapreceptúra sósavlehasadás vizsgálata 170 °C-on

Plasticised PVC becomes more resistant to high temperatures after of Oxydtron addition, as shown in *Fig. 5* which represents the dehydrochlorination results of plasticised PVC containing 1% Oxydtron at 170 °C; where the slope of the conversion rate curve decreased from (0.000134) in case of plasticised PVC basic formulation (without additive) to (0.000073) after Oxydtron addition, where the tendency of plasticised PVC to release chlorine containing compounds has been reduced and increased thermal stability and degradation resistance accompanied by extended degradation time range for plasticised PVC basic formulation from (2.21 hours) to (4.75 hours) after 1% Oxydtron addition. When the weight fraction of Oxydtron additives increases the thermal resistance stability of plasticised PVC will rise and this behavior can be distinguished by the *Fig. 6* and *Fig. 7* which represent the dehydrochlorination results of plasticised PVC containing 3% and 5% Oxydtron at 170 °C respectively. From these figures, we notice that the slope of conversion rate curve will decrease, i.e. the degradation resistance has been increased, where in case of of 3% Oxydtron content the slope of conversion rate curve becomes (0.000062) with an increase in the total degradation time to (4.84 hours), and in case of of 5% Oxydtron content the slope of conversion rate curve will reduce to (0.000053) and increasing the total degradation time to (5.20 hours).

From *Fig. 8* which represent the Dynamic Mechanical Analysis (DMA) for plasticised PVC-Oxydtron hybrid composite, we can note that the Oxydtron additives increase the glass transition temperature (Tg), where the glass transition temperature shifts to higher temperatures rising from (-3.26 °C) in case of plasticised PVC basic formulation to (0.30 °C) when 1% of Oxydtron has been added and continues to rise to (3.50 °C) and (4.66 °C) when added 3% and 5% of Oxydtron respectively. Clearly, there is an interaction between

PVC and Oxydtron molecules, which causes the reduction of kinetic energy of plasticised PVC, and reducing the segmental movement, which probably prevents the molecules from assembling in crystalline systems, so the relaxation time of this movement increases. So the polymer will consist of long physically crosslinked liquid-like molecules [30].

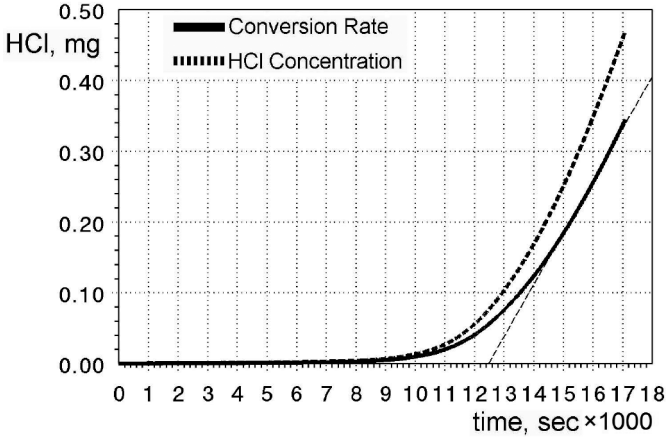

Fig. 5 Dehydrochlorination results of plasticised PVC containing 1% Oxydtron at 170 °C
5. ábra Az 1% Oxidtron tartalmú lágy PVC sósavlehasadás vizsgálata 170 °C-on

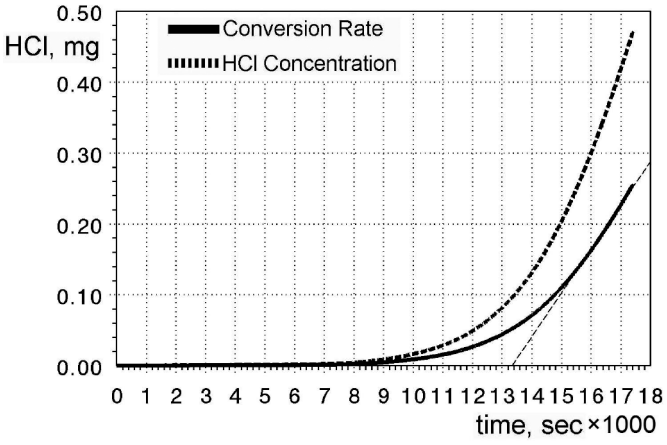

Fig. 6 Dehydrochlorination results of plasticised PVC containing 3% Oxydtron at 170 °C
6. ábra A 3% Oxidtron tartalmú lágy PVC sósavlehasadás vizsgálata 170 °C-on

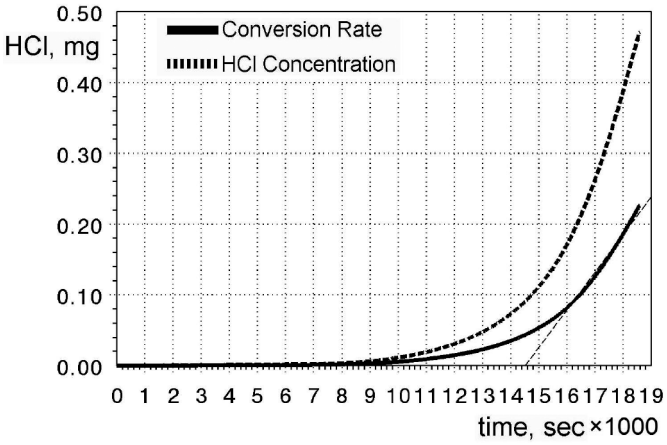

Fig. 7 Dehydrochlorination results of plasticised PVC containing 5% Oxydtron at 170 °C
7. ábra Az 5% Oxidtron tartalmú lágy PVC sósavlehasadás vizsgálata 170 °C-on

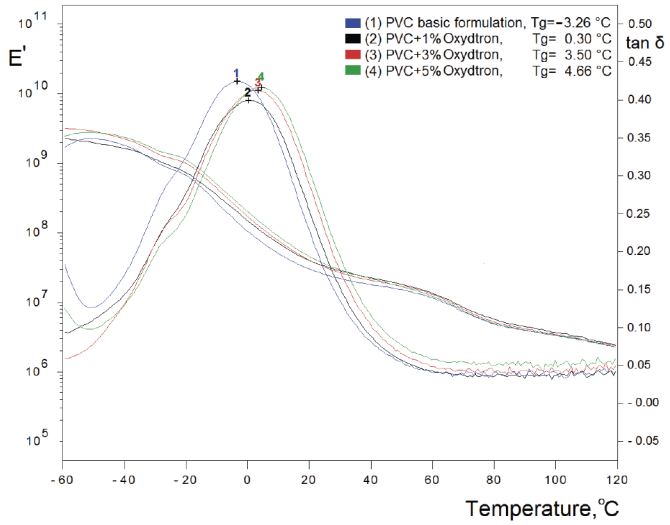

Fig. 8 Dynamic mechanical analysis for plasticised PVC-Oxydtron hybrid composite
8. ábra A lágy PVC – Oxidtron hybrid kompozitok dinamikus mechanikai analízise

5. Conclusions

In general, Oxydtron improves the thermal properties of plasticised PVC, where the enhancement of L.O.I value reached to (22.22%) at 5% Oxydtron content. The degradation rate of plasticised PVC also decreased after adding Oxydtron, where the improvement of time required for total degradation with plasticised PVC containing 5% Oxydtron was (135.30%) longer than plasticised PVC basic formulation. Glass transition temperature was shifted towards higher temperatures after Oxydtron addition, and this indicates that Oxydtron directly affects kinetic energy and segmental movement of plasticised PVC causing to decrease them.

References

[1] Al-Mosawi, A.I. – Marossy, K. (2018): Heat effected zone in unburned, antimony trioxide containing plasticized poly(vinyl chloride), Építőanyag-Journal of Silicate Based and Composite Materials, Vol.70, No.3, pp.86-89. https://doi.org/10.14382/epitoanyag-jsbcm.2018.16

[2] Dowden, K. (2016): Prometheus, Oxford Research Encyclopedias. https:// 10.1093/acrefore/9780199381135.013.5363

[3] Al-Mosawi, A.I. (2016): Flammability of Composites, Chapter 14 in J. Njuguna (ed.) Lightweight composite structures in transport: Design, manufacturing, analysis and performance, Woodhead Publishing, UK, pp. 361-369. https://doi.org/10.1016/B978-1-78242-325-6.00014-1

[4] Al-Mosawi, A.I. – Rijab, M.A. – Salaman, A.J. – Alwash, N.A. – Aziz, N.S. (2012): Flammability Behavior of Composite Mixed with Retardant Agents, Applied Mechanics and Materials, Vol. 186, pp. 129-131. https://doi.org/10.4028/www.scientific.net/AMM.186.129

[5] Al-Maamori, M.H. – Al-Mosawi, A.I. – Hashim, A.A. (2011): Flame Retardancy Enhancement of Hybrid Composite Material by Using Inorganic Retardants, Materials Sciences and Applications, Vol.2, No.8, pp. 1134-1138. https://doi.org/10.4236/msa.2011.28153

[6] Al-Mosawi, A.I. – Ahmed, J.K. – Hussain, H.A. (2012): Evaluation Flame Retardancy of Epoxy Composite by Using Design of Experiments, Applied Mechanics and Materials, Vol. 186, pp. 156-160. https://doi.org/10.4028/www.scientific.net/AMM.186.156

[7] Brushlinsky, N. – Ahrens, M. – Sokolov, S. – Wagner, P. (2016): World fire statistics, Report No.21, International association of fire and rescue services, Center of fire statistics.

[8] Fire Research Report (2012): Comparison of European Fire Statistics, Final report for the Department for Communities and Local Government, Eland House, London, UK.

[9] Winberg, D. (2016): International Fire Death Rate Trends, SP Technical Research Institute of Sweden, Report No.32.

[10] Al-Mosawi, A.I. – Marossy K. (2019): Effect of Extrusion Speed and ATO Content on Rheological Properties of Plasticised PVC, IOP Conf. Ser.: Mater. Sci. Eng., Vol.613, pp.1-5 (012029). https://doi.org/10.1088/1757-899X/613/1/012029

[11] Al-Mosawi, A.I. – Marossy, K. (2019): Processing Conditions and Their Effect on Homogeneity of PPVC Structural Characteristics, ARPN Journal of Engineering and Applied Sciences, Vol.14, No.14, pp.2485-2491.

[12] Al-Mosawi, A.I. – Marossy, K. (2018): Performance Evaluation of Mixing Mechanism and its Effects on Thermal Behaviour of Plasticised PVC, International Journal of Engineering and Technology (IJET),Vol. 9,No. 6, pp.4389- 4396. https://doi.org/10.21817/ijet/2017/v9i6/170906130

[13] Al-Mosawi, A.I. – Marossy, K. – Kónya, C. (2018): Effect of Plasticizer Percentage on Thermal Properties of Plasticised PVC, Elixir International Journal,Vol. 117,pp.50509-50511.

[14] Al-Mosawi, A.I. – Al-Zubadi, A.A. – Al-Maamori , M.H. – Al-Maimuri, N.M. (2013): Fire Retardants for Civil Structures, Global Journal of Researches in Engineering: C, Chemical Engineering, Vol.13, Issue.2, pp. 8-12.

[15] Hull, T.R. – Witkowski, A. – Hollingbery, L. (2011): Fire Retardant Action of Mineral Fillers, Polymer Degradation and Stability, Vol.96, Issue.8, pp.1462-1469. https://doi.org/10.1016/j.polymdegradstab.2011.05.006

[16] Li, M. – Zhang, J. – Huang, K. – Li, S. – Jianga, J. – Xia, J. (2014): Mixed Calcium and Zinc Salts of Dicarboxylic Acids Derived from Rosin and Dipentene: Preparation and Thermal Stabilization for PVC, RSC Advances, Vol.4, 2014, pp.63576-63585. https://doi.org/10.1039/C4RA10657A

[17] Jiao,Y. – Wang, X. – Peng, F. – Xu, J. – Gao, J. – Meng, H. (2014): Increased Flame Retardant, Smoke Suppressant and Mechanical Properties of Semi-Rigid Polyvinyl Chloride (PVC) Treated with Zinc Hydroxystannate Coated Dendritic Fibrillar Calcium Carbonate, Journal of Macromolecular Science, Part B: Physics, Vol.53, Issue.3, pp.541-554. https://doi.org/10.1080/00222348.2013.852061

[18] Asawakosinchai, A. – Jubsilp, C. – Mora, P. – Rimdusit, S. (2017): Organic Heat Stabilizers for Polyvinyl Chloride (PVC): A Synergistic Behavior of Eugenol and Uracil Derivative, Journal of Materials Engineering and Performance, Vol.26, Issue.10, pp.4781-4788. https://doi.org/10.1007/s11665-017-2923-0

[19] Liu, P. – Zhao, M. – Guo, J. (2006): Thermal Stabilities of Poly(Vinyl Chloride)/Calcium Carbonate (PVC/$CaCO_3$) Composites, Journal of Macromolecular Science, Part B: Physics, Vol.45, Issue.6, pp.1135-1140. https://doi.org/10.1080/00222340600962650

[20] Grossman, R.F. (2008): Handbook of Vinyl Formulating, 2nd edition, Wiley series on plastics engineering and technology, John Wiley & Sons, Inc. publication, New Jersey USA. https://doi.org/10.1002/9780470253595

[21] Bioekotech (2014): Oxydtron Nanocement, Cement Quality Improving Admixture, BIOEKOTECH Hungary KFT.

[22] Dunuweera, S.P., Rajapakse, R.M.G. (2018): Cement Types, Composition, Uses and Advantages of Nanocement, Environmental Impact on Cement Production, and Possible Solutions, Advances in Materials Science and Engineering, Vol.2018, pp. 1-11 (ID 4158682). https://doi.org/10.1155/2018/4158682

[23] Merlin, F. – Lombois, H. – Joly, S. – Lequeux, N. – Halary, J. – Van Damme, H. (2002): Cement-Polymer and Clay-Polymer Nano- and Meso-Composites: Spotting the Difference, Journal of Materials Chemistry, Vol. 12, No. 11, pp. 3308-3315. https://doi.org/10.1039/B205279M

[24] ISO 4589-2 (2017): Plastics - Determination of burning behavior by oxygen index - Part 2: Ambient-temperature test, International Organization for Standardization (ISO).

[25] ISO 182-3 (1993): Plastics-Determination of the tendency of compounds and products based on vinyl chloride homopolymers and copolymers to evolve hydrogen chloride and any other acidic products at elevated temperatures-Part 3: Conductometric method, International Organization for Standardization (ISO).

[26] ISO 6721-11 (2012): Plastics-Determination of dynamic mechanical properties - Part 11: Glass transition temperature, International Organization for Standardization (ISO).

[27] Hobbs, C.E. (2019): Recent Advances in Bio-Based Flame Retardant Additives for Synthetic Polymeric Materials, Polymers, Vol. 11, Issue.2, pp. 1-31. https://doi.org/10.3390/polym11020224

[28] Al-Mosawi, A.I., Marossy, K. (2018): L.O.I and DSC Analyses of Antimony Trioxide Containing Plasticized PVC as a Function of Processing Method, MultiScience - XXXII. microCAD International Multidisciplinary Scientific Conference, University of Miskolc, Hungary, 5-6 September, pp.1-5. https://doi.org/10.26649/musci.2018.017

[29] Zheng, X-G., Tang, L-H., Zhang, N., Gao, Q-H., Zhang, C-F., Zhu, Z-B. (2003): Dehydrochlorination of PVC Materials at High Temperature, Energy and Fuels, Vol.17, Issue.4, pp. 896-900. https://doi.org/10.1021/ef020131g

[30] Marossy, K. (2006): Testing polymer mixtures by Dynamic Mechanical Analysis, Manuscript of a lecture: Hungarian Academy of Sciences.

Ref.:
Al-Mosawi, A.I. – **Marossy**, Kálmán: *Thermal stability and flame retardant properties of plasticized poly(vinyl chloride) hybrid composite for construction application*
Építőanyag – Journal of Silicate Based and Composite Materials, Vol. 71, No. 6 (2019), 198–203. p.
https://doi.org/10.14382/epitoanyag-jsbcm.2019.35

Rheology of natural hydraulic lime pastes modified by non-traditional biopolymeric admixtures

Tomáš ŽIŽLAVSKÝ ▪ Institute of Chemistry, Faculty of Civil Engineering, Brno University of Technology, Czech Republic ▪ zizlavsky.t@fce.vutbr.cz

Martin VYŠVAŘIL ▪ Institute of Chemistry, Faculty of Civil Engineering, Brno University of Technology, Czech Republic ▪ vysvaril.m@fce.vutbr.cz

Pavla ROVNANÍKOVÁ ▪ Institute of Chemistry, Faculty of Civil Engineering, Brno University of Technology, Czech Republic ▪ rovnanikova.p@fce.vutbr.cz

Érkezett: 2019. 11. 29. ▪ Received: 29. 11. 2019. ▪ https://doi.org/10.14382/epitoanyag-jsbcm.2019.36

Abstract

Viscosity enhancing admixtures, widely used to improve characteristics of concrete and ready-mix mortars, are mainly different derivatives of cellulose. Due to the nature of cellulose processing, the environmental-friendlier alternatives should be studied in order to reduce the impact of the building industry on the environment. The rheological study of natural hydraulic lime (NHL) grouts modified by four different biopolymers is carried out to investigate their behaviour in the NHL-based mortars.

The biopolymers studied are of seaweed (sodium salt of alginic acid (ALGNA) and carrageenan (CG)) and microbial (diutan gum (DG) and xanthan gum (XG)) origin. The effect of addition of these admixtures in the doses of 0.1%, 0.5%, and 1% was studied using hybrid rheometer with DIN concentric cylinders geometry. The flow properties as well as viscoelastic properties were studied. The addition of any of the admixtures led to the increase in yield stress, with DG being the most effective admixture. Desirable increase in consistency coefficient was observed within the pastes with CG and DG addition having growing dosage dependency, the ALGNA addition also increased the coefficient noticeably, but it was furtherly decreased with growing dose of admixture. The fluidity index lower than 1 expressed shear-thinning behaviour of studied pastes, except the pastes with highest dose of admixtures, and all of the XG pastes. The addition of CG and DG supported the stability of the grout expressed as the increase in critical strain, thus prolongation of linear viscoelastic region. The flow strain was increased by all of the studied admixtures promoting the gel-like behaviour of the pastes. Complex modulus and viscosity measured at 1Hz frequency were unaffected by the DG addition while they were increased notably by addition of other admixtures with ALGNA and XG supporting the resistance to deformation of the grouts studied. Correspondingly to complex modulus increase, the loss tangent is diminished, reporting more elastic behaviour of the material.

All of the admixtures studied increased the yield stress, and the influence of most of them had similar trends within other properties. Noticeable differences in efficiency and dosage-dependency were observed. The xanthan gum was overall the worst performing admixture. This was mainly due to higher sensitivity of xanthan to the concentration of bivalent ions in the solution.

Keywords: natural hydraulic lime, rheology, flow properties, viscoelastic properties, biopolymeric admixture

Kulcsszavak: természetes hidraulikus mész, reológia, folyási tulajdonságok, viszkoelasztikus tulajdonságok, biopolimer keverék

Tomáš ŽIŽLAVSKÝ
has graduated at Faculty of Civil Engineering (FCE), Brno University of Technology (BUT) (2017) in the field of materials engineering. Continues as a PhD student at the Institute of chemistry, FCE, BUT with the main interest in lime grouts, mortars and their modifications.

Martin VYŠVAŘIL
has PhD in inorganic chemistry, Faculty of Science, Masaryk University (2009). Currently assistant professor at the Institute of Chemistry, FCE, BUT. Specialized on the Chemistry of building materials, mainly investigation in modification and utilization of gypsum, rehydration of cement past after heating, sulfate attack on concrete, development of new materials based on cement and lime with using the secondary raw materials and lightweight aggregate investigation in rheology of building materials.

Pavla ROVNANÍKOVÁ
a professor at Institute of chemistry, FCE BUT. Specializes on the chemistry of building materials mainly historical binders, especially plasters of build heritage, pozzolanic materials, degradation of lime-based materials, degradation of concrete, and alkali-activated aluminosilicates

1. Introduction

The viscosity enhancing admixtures (VEAs) are used to modify the fresh state properties of building materials, mainly plasters and self-consolidating concrete (SCC) [1, 2]. The VEAs are often of polysaccharidic origin, currently most used are cellulose ethers, but a range of natural gums (e.g. welan gum, guar gum, gum arabic, etc.) is being studied. This study is focused on two biopolymers of microbial origin (xanthan (XG) and diutan gum (DG)), and two obtained from seaweeds (sodium salt of alginic acid (ALGNA) and carrageenan (CG)). These VEAs have been scarcely studied for the use in cementitious material, especially in SCC, and are mainly used in the food industry as gelling and thickening agents and stabilisers [2–4].

The microbial XG and DG are partially in use in building industry, where they reduce segregation and bleeding of SCC mixtures [2, 3, 5]. Xanthan gum, with slump-reducing side effect in utilization in SCC, proposes shear-thinning behaviour [6] in cementitious compositions [2, 7]. While used in the aerial lime-based [8, 9] mortars, the efficiency of XG addition was lower than the expectations based on the results from cement mixtures. This discrepancy is probably caused by a cationic sensitivity of XG, especially in the case of bivalent (e.g. Ca^{2+}) ions [10]. In the other types of materials, xanthan gum based stabilizer has been successfully used to improve the stability of fly ash-metakaolin geopolymer binary system [11]. The DG is of similar use and properties to XG with even less sensitivity to the conditions such as pH, temperature and salinity [10, 12]. DG is more efficient in the modifying of rheological properties

of aqueous solution, thus having more dosage-dependent effect [10]. The improved stability of SCC by the DG addition is achieved by the increase in yield stress of the mixture [1]. The ALGNA, acquired from brown seaweed, has properties comparable with the commercially available super-absorbent polymers (SAP) [13]. The impure brown seaweed extract, containing 10–40% of dry weight of alginates was used by León-Martínez et al. as a VEA for SCC with interesting results, the properties of the extract are comparable with the pure sodium alginate, especially in higher concentrations, both, the sodium alginate as well as algae extract express the shear-thinning behaviour of aqueous dispersions [14]. The addition of sodium alginate to either aerial or hydraulic lime mortar leads to the increase in yield stress and promotion of shear-thickening behaviour of the pastes [8, 15]. Carrageenan (CG) is, as well as more famous gelling agent agar, obtained from red seaweed. There exists a wide range of carrageenan types with different degree of sulfatation, which influences mainly the solubility and gel strength [16]. The CG addition improves the mechanical properties of fly-ash based geopolymers, mainly by creating more condensed structure [17, 18]. The short-term strengths of lime mortars have not been notably improved in the case of hydraulic lime [19] and significantly decreased in the case of aerial lime [9], but with the difference diminishing with further ageing. The aerial lime pastes rheology is improved by increase in yield stress and consistency coefficient, and also by prolongation of period of gel-like behaviour observed by study of viscoelastic properties.

The presented paper studies the influence of the above-mentioned biopolymers on the flow and viscoelastic properties of natural hydraulic lime (NHL) based grouts focusing on the dosage-dependency of the biopolymer addition.

2. Materials and methods

2.1 Materials and sample preparation

All the grouts studied were prepared by dry mixing of natural hydraulic lime of NHL 3.5 class according to EN 459-1 (Zement- und Kalkwerke Otterbein GmbH & Co. KG, Germany) and biopolymeric admixture (summary of admixtures used, and their characteristics are stated in *Table 1*) in the dosage of 0.1%, 0.5%, and 1% of the binder weight. Water was then added using constant water:binder ratio of 0.7 and the paste was prepared by mixing for one minute. The grout was then introduced into measuring cup of Discovery HR-1 hybrid rheometer by TA instruments using DIN concentric cylinders measuring geometry tempered to 20°C. The measurement was started by a 60 s preshear at 100 s^{-1}, which begun 5 minutes after water introduction into the dry mixture, followed by 60 s resting time. The curves were analysed using TRIOS 4.0.2.30774 software.

2.2 Methods of measurement

The measuring procedure has been described in detail in previous publication [8], thus only the basic description follows.

Abbrev.	Chemical composition	Commercial name	Viscosity (1% aq. solution, 20°C) [mPa s]	Manufacturer
ALGNA	sodium alginate	–	14.5	Sigma-Aldrich, Co.
CG	carrageenan	Genuvisco CG–131	72.1	CP Kelco
DG	diutan gum	Kelco-Crete DG–F	13 363.8	CP Kelco
XG	xanthan gum	Kelzan AP–AS	7 633.3	CP Kelco

Table 1 Abbreviations, characteristics, and producers of the admixtures used
1. táblázat Az alkalmazott adalékszerek jelölése, jellemzői és gyártói

2.2.1 Flow properties

The results obtained by procedure described in [8] were expressed graphically as flow curves (shear rate vs shear stress) and the downward curves were analysed using Hershel-Bulkley model (Eq. 1) to obtain the variables describing behaviour of the samples.

$$\tau = \tau_0 + k\dot{\gamma}^n \quad (1)$$

where τ - shear stress, $\dot{\gamma}$ - shear rate, τ_0 - yield stress, k consistency coefficient and n - fluidity index which characterizes shear-thinning ($n < 1$) or shear-thickening ($n > 1$) behaviour of a material.

2.2.2 Viscoelastic properties

To determine the length of linear viscoelastic region (LVR), characterized by the critical strain γ_C, and flow point γ_F, described as the equilibrium between loss (G') and storage (G'') modulus, the small amplitude oscillation test at 1 Hz frequency was carried out. The strain value from the LVR of all samples was chosen to execute the frequency sweep test (0.1 Hz – 10 Hz) in linear conditions. The results were expressed as complex modulus G^* and loss tangent tan (δ) as defined by equations 2 and 3 respectively.

$$G^* = \sqrt{(G')^2 + (G'')^2} \quad (2)$$

$$\tan(\delta) = G''/G' \quad (3)$$

3. Results and discussion

3.1 Flow properties

The measurement data were expressed as shear rate vs shear stress diagram. For the illustrational purposes, the downward curves of pastes with ALGNA addition are shown in *Fig. 1*. The transition from pseudoplastic (shear-thinning, $n < 1$) to dilatant (shear-thickening, $n > 1$) behaviour is observed as a change of shape of curves from convex (REF, ALGNA 0.1% and 0.5%) to concave (ALGNA 1%). The values of yield stress (τ_0), consistency coefficient (k), and fluidity index (n) for all the pastes are compared in *Fig. 2*. The admixture addition increases the yield stress of pastes with further growth with increasing dosage, which is typical for the VEAs in traditional building materials [8, 9, 20–22]. The non-monotonicity of CG and XG addition was observed and described by Cappellari et al. [20] on the cementitious mortars modified by hydroxypropyl

guaran (HPG) and methylhydroxyethyl cellulose, and it is also reported on the NHL pastes modified by HPG with low degree of substitution and hydroxypropyl methyl cellulose [9]. The non-monotonicity is supposed to be caused by the competition between the lubricating and dispersing effect of the admixtures [20]. The most effective admixtures in the lowest dose are CG and XG, while DG is the most efficient admixture in higher doses. The increase in consistency coefficient (k) is connected with improvement of adhesive and anti-sagging properties of grouts. The reversed dosage-dependency of ALGNA is contrary to the aerial lime results [8], and also the inefficiency of XG is much clearer. The extreme drop of k value for CG and DG in highest dosage is probably caused by the high thickness of the tested samples. Lower doses of ALGNA and CG, as well as DG, may be potentially beneficial for the use to modify e.g. tile adhesives. The value of fluidity index, as stated earlier, describes whether the mixture's behaviour is shear-thinning or shear-thickening. The shear-thinning behaviour is more common and mostly desired in the case of building materials [8, 9, 15]. The transition from shear-thinning to shear-thickening behaviour is due to water-retentive function of biopolymers [9] that causes a decrease in liquid phase content in the grout, which is basically a suspension of NHL particles in water/water-biopolymer environment, thus the paste draws to the state of "thick suspensions of particles in a liquid", which is the typical example of dilatant fluid [23]. The alginate and DG addition in lower dosage promotes the shear-thinning behaviour of the paste, while high doses of biopolymers and XG in general promote dilatancy of the pastes. A. Azzizi and P. F. G. Banfill [15] observed an opposite trend with the ALGNA addition but using much lower concentrations. Based on the comparison of the two results, it can be assumed that somewhere between the dosage of 0.035% (the highest dose in [15]) and 0.5% of binder weight lies a dose of alginate, at which the thixotropy of the NHL based paste is the most promoted. The studied biopolymers behave differently in comparison to hydroxypropyl derivatives of guar gum, chitosan or cellulose [24] (the same experimental setup on the same measuring device).

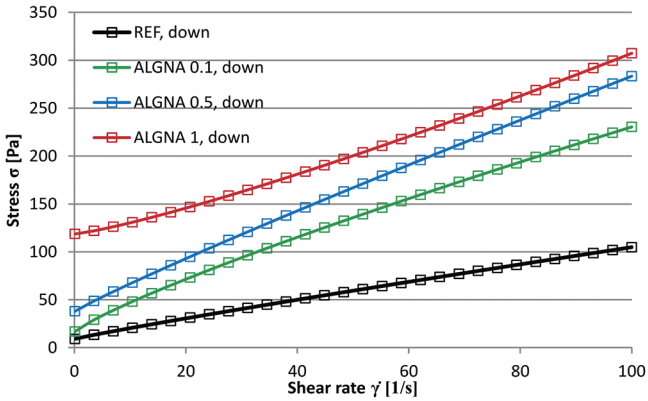

Fig. 1 Downward flow curves of NHL pastes modified by different amount of ALGNA

1. ábra Eltérő mennyiségű ALGNA-val módosított NHL pépek folyási görbéi

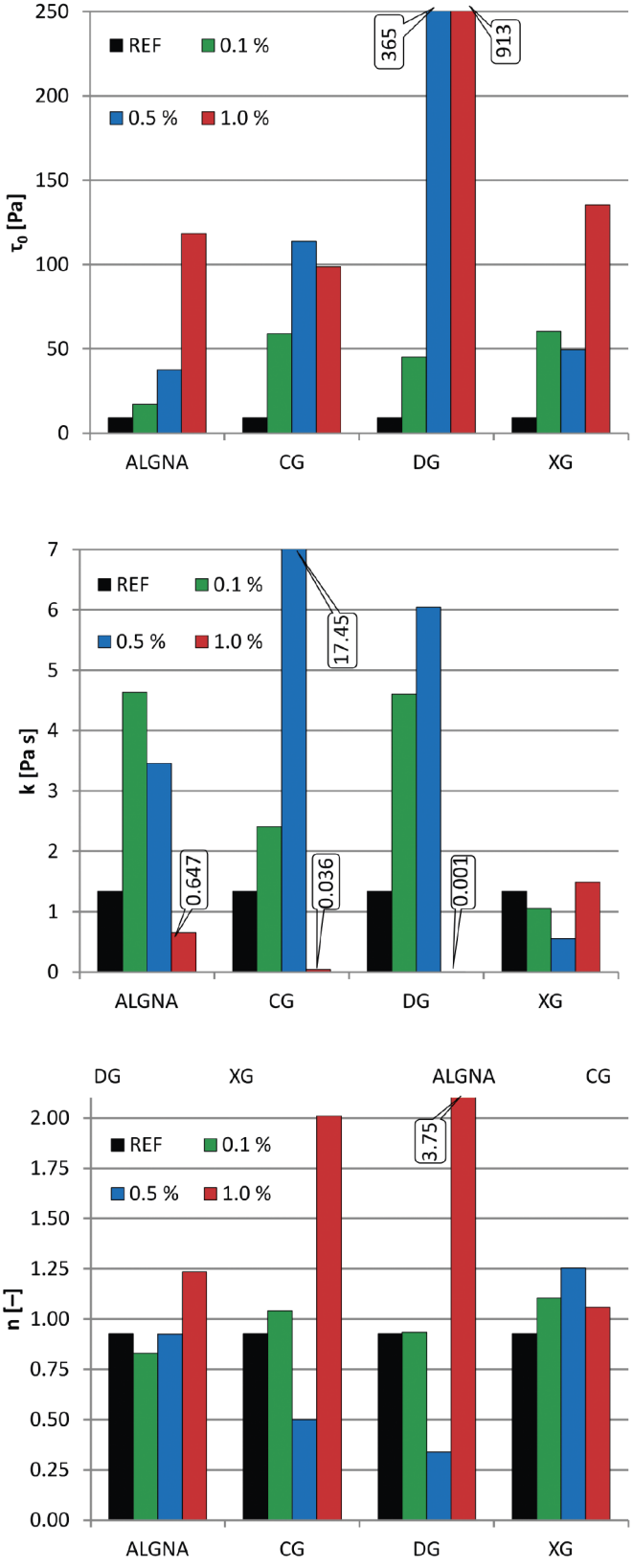

Fig. 2 Comparison of yield stress (τ_0), consistency coefficient (k), and fluidity index (n) of NHL-based pastes modified by biopolymers

2. ábra Biopolimerekkel módosított NHL alapú pépek folyási feszültsége (τ_0), konzisztencia együtthatója (k), and folyékonysági mutatója (n)

3.2 Viscoelastic properties

3.2.1 Amplitude sweep test

The critical strain γ_C determines the length of LVR, thus also the stability of the paste (the longer the LVR, the more stable the paste). The moduli curves in the modulus/oscillation strain system for ALGNA, alongside with the examples of the critical and flow strain values (γ_C and γ_F respectively) are shown in *Fig. 3*, while in *Fig. 4*, the strain values for all mixtures are compared. The addition of CG and DG in lowest dose do not affect the value of critical strain, which is furtherly increased with growing dosage of admixture, whereas the CG is more efficient in the dosage of 1%. This behaviour is similar to the one of hydroxypropyl derivatives of guaran, chitosan and cellulose [24], out of which cellulose ether are currently one of the most common VEAs used. The ALGNA decreases the value of γ_C, thus the ALGNA-modified pastes behave differently than cementitious pastes modified by marine brown algae extract in which the alginates are present [14]. The XG slightly decreases grouts stability in low dosage and improves it with growing dosage, which is in correspondence with the behaviour of XG aqueous solution in different concentrations [6].

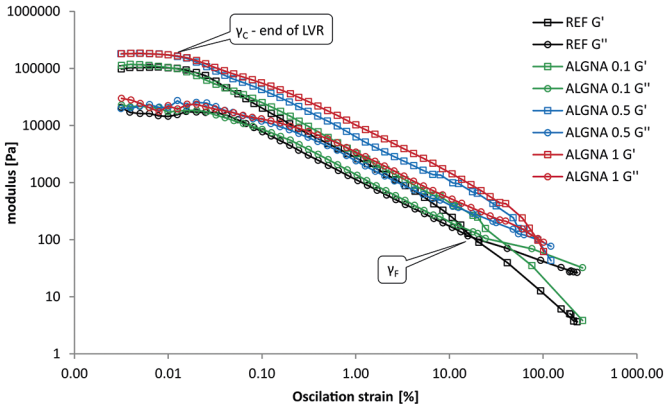

Fig. 3 Storage modulus (G') and Loss modulus (G") of pastes with ALGNA addition
3. ábra ALGNA hozzáadásával készült pépek tárolási (G') és veszteségi modulusa (G")

The second parameter studied, the flow strain γ_F, marks the point of transition from solid viscoelastic behaviour (G' > G") to liquid behaviour (G' < G"). The addition of admixtures markedly increases the flow strain value as seen in *Fig. 4*. In the case of CG and DG, the highest increase is within the lowest dosage (0.1%) and with growing dosage, the flow strain value decreases. This trend is similar to hydroxypropylmethyl cellulose (HPMC) and hydroxypropyl guaran (HPG) [24] on the same instrumental setup but CG and DG seem to be more efficient. In the case of DG 0.1% the moduli did not intersect in the studied strain range, thus the paste retains viscoelastic properties. The growth of γ_F for ALGNA up until dosage of 0.5% is in accordance with results of León-Martínez et al [14], where the increase in flow stress was observed. The XG is in efficiency of affecting the γ_F inferior to the three other admixtures with unclear dosage-dependency.

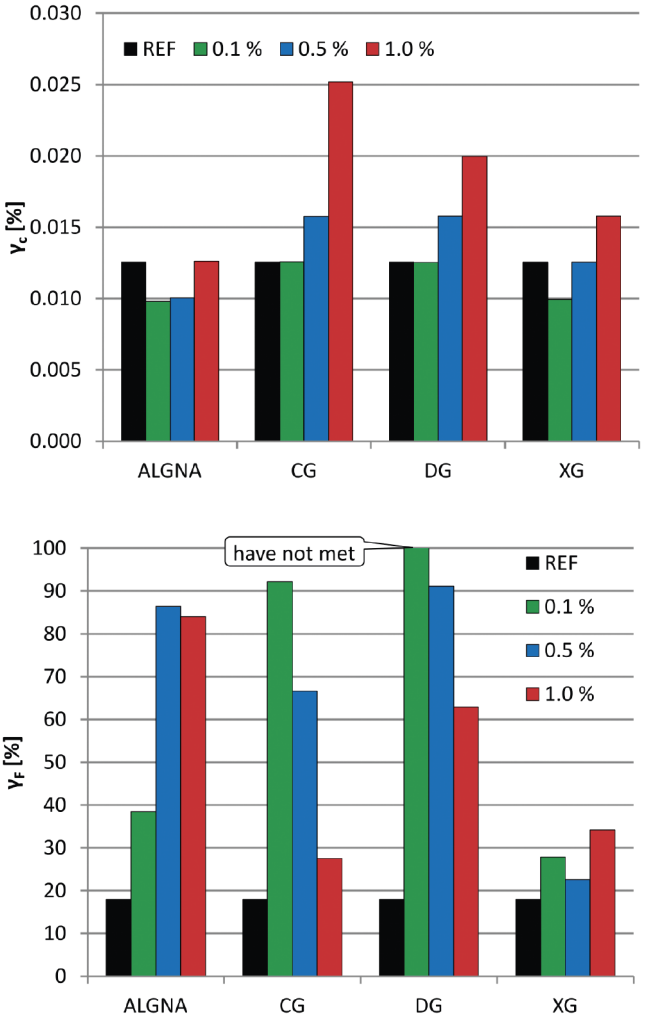

Fig. 4 Comparison of critical strain (γ_C) and flow strain (γ_F) values of tested samples
4. ábra A vizsgált minták kritikus deformációja (γ_C) és folyási deformációjának (γ_F) összehasonlítása

3.2.2 Flow sweep test

The test was carried out at 0.005% strain, which ensures that all the pastes are in the LVR. The data obtained were visualised using charts similar to *Fig. 5* and the values of complex shear modulus (G^*), and loss tangent (tan (δ)) at 1 Hz frequency were recorded for comparison and are presented in *Fig. 6*. The growth of resistance to deformation of the samples represented by increasing value of G^* in combination with decrease in loss tangent corresponds with the results of amplitude sweep tests. The values of tan (δ) indicate prevailing elastic behaviour of samples with storage modulus being 4-10 times higher than loss modulus. The extremely low tan (δ) value of DG 0.1 % may be interpreted as behaviour of ideally elastic material. The decrease in loss tangent with addition of VEA has been observed also with HPG and chitosan derivatives in lime mortars [25, 26], and hydroxypropyl derivatives of several biopolymers in NHL pastes [24]. On the other hand, HPG and HPMC in cementitious paste did not cause a decrease and starch ether in initial dose caused increase in loss tangent [20]. The gradual increase in tan (δ) with growing dosage, observed especially in the case of CG and DG where the trend

corresponds with the growth of flow strain, is also described in aforementioned literature within different admixtures in several binder systems. The studied biopolymers, previously used in aerial-lime pastes [8], exhibited opposite trends in both binder systems, with exception of XG, where the trends are unclear in both cases.

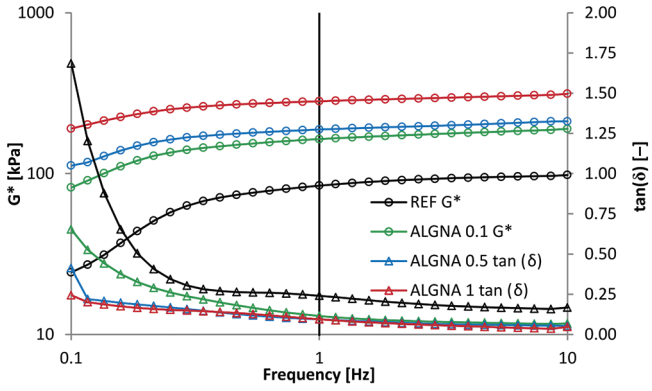

Fig. 5 Results of frequency sweep test for NHL paste with ALGNA
5. ábra ALGNA hozzáadásával készült NHL pépek frekvenciaáram vizsgálatának eredményei

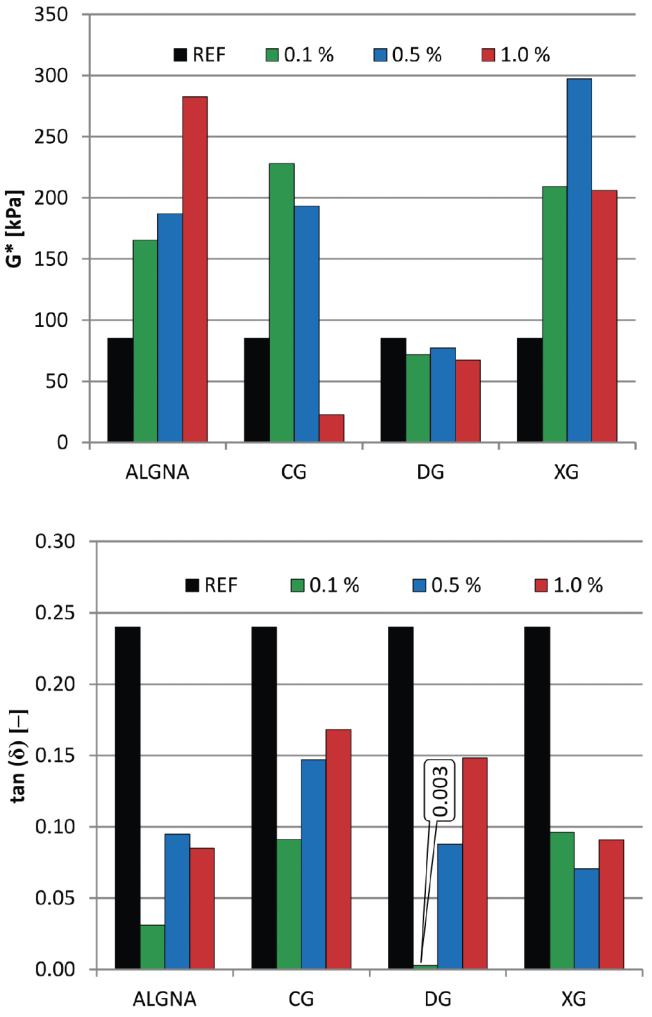

Fig. 6 Complex modulus (G) and loss factor (tan (δ)) comparison of tested pastes*
6. ábra A tesztelt minták komplex modulusának (G) és veszteség tényezőjének (tan (δ)) összehasonlítása*

4. Conclusion

The study informs about influence of addition of biopolymeric admixtures on the rheological properties of natural hydraulic lime pastes.

The addition of biopolymers increased the yield stress of the pastes with growing dosage dependency. The sodium salt of alginic acid, carrageenan and diutan gum increased the consistency coefficient, which is connected with adhesive and anti-sagging properties of mixture, but alginate had dosage-dependency trend opposite to the other two admixtures. Addition of these three biopolymers in the dosage of 1% lead to transition of the behaviour of the pastes from pseudoplastic to dilatant, while xanthan gum modified paste showed shear thickening characteristics even in the lowest dose of 0.1%. The study on viscoelastic properties of the modified pastes showed improvement of stability of the grouts modified by carrageenan and diutan gum by prolonging the linear viscoelastic region. The promotion of gel-like behaviour has been observed for all biopolymers but xanthan gum was inferior in efficiency to the other three admixtures. The beneficial effect of the admixtures on the stability of the grouts was also observed by flow sweep tests. The values of complex strain modulus and especially loss tangent support the conclusions.

The use of xanthan gum in natural hydraulic lime pastes is limited due to low efficiency and unclear trends within some of the studied properties. The diutan gum and carrageenan were the admixtures which showed the greatest similarity in behaviour with the hydroxymethylpropyl cellulose, one of the most spread viscosity enhancing admixture in commercial use.

Acknowledgement

The work was financially supported by the BUT specific research project FAST-J-19-5803.

References

[1] Van Der Vurst, F. – Grünewald, S. – Feys, D. – Lesage, K. – Vandewalle, L. – Vantomme, J. – De Shutter, G. (2017): Effect of mix design on the robustness of fresh self-compacting concrete. Cem Concr Compos 82. http://dx.doi.org/10.1016/j.cemconcomp.2017.06.005

[2] Plank, J., (2004) Application of biopolymers and other biotechnological products in building materials. Appl Microbiol Biotechnol 66. http://dx.doi.org/ 10.1007/s00253-004-1714-3

[3] Singh, N. K. – Mishra, P.C. – Singh, V.K. – Narang, K.K. (2003) Effects of hydroxyethyl cellulose and oxalic acid on the properties of cement. Cem Concr Res. 33. http://dx.doi.org/10.1016/S0008-8846(03)00060-7

[4] Rinaudo, M. (2008) Main properties and current applications of some polysaccharides as biomaterials. Polym Int 57. http://dx.doi.org/10.1002/pi.2378

[5] Isik, I.E. – Ozkul, M.H. (2014) Utilization of polysaccharides as viscosity modifying agent in self-compacting concrete. Constr Build Mater 72, http://dx.doi.org/10.1016/j.conbuildmat.2014.09.017

[6] Martín-Alfonso, J.E. – Cuadri, A.A. – Berta, M. – Stading, M. (2018) Relation between concentration and shear-extensional rheology of xanthan and guar gum solutions. Carbohydr Polym 181. http://dx.doi.org/10.1016/j.carbpol.2017.10.057

[7] Vazquez, A. – Pique, T.M. (2016), Biopolymers and Biotech Admixtures for Eco-Efficient Construction Materials, Woodhead Publishing, Duxford, .

[8] Žižlavský, T. – Vyšvařil, M. – Rovnaníková, P. (2018) Rheological characteristics of aerial lime-based pastes with biopolymers. IOP Conf Ser Mater Sci Eng 385 http://dx.doi.org/10.1088/1757-899X/385/1/012067

[9] Žižlavský, T. – Vyšvařil, M. – Rovnaníková, P. (2018) Characterization of aerial lime-based mortars with addition of biopolymers. IOP Conf Ser Mater Sci Eng 379 http://dx.doi.org/ 10.1088/1757-899X/379/1/012006
[10] Xu, L. – Gong, H. – Dong, M. – Li, Y. (2015) Rheological properties and thickening mechanism of aqueous diuta gum solution: Effects of temperature and salts. Carbohydr Polym. 132 http://dx.doi.org/10.1016/j.carbpol.2015.06.083
[11] Aboulayt, A. – Jaafri, R. – Samouh, H. – Cherki El Idrisi, A. – Roziere, E. – Moussa, R. – Loukili, A. (2018) Stability of new geopolymer grout: Rheological and mechanical performances of metakaolin-fly ash binary mixtures. Constr Build Mater. 181 http://dx.doi.org/10.1016/j.conbuildmat.2018.06.025
[12] Xu, L. – Qiu, Z. – Gong, H. – Zhu, C. – Li, Z. – Li, Y. – Dong, M. (2019) Rheological behaviors of microbial polysaccharides with different substituents in aqueous solutions: Effects of concentration, temperature, inorganic salt and surfactant. Carbohydr Polym 219. http://dx.doi.org/10.1016/j.carbpol.2019.05.032
[13] Mignon, A. – Snoeck, D. – D'Halluin, K. – Balcaen, L. – Vanhacke, F. – Dubruel, P. – Van Vlierberghe, S. – De Belie, N. (2016) Alginate biopolymers: Counteracting the impact of superabsorbent polymers on mortar strength. Constr Build Mater 110 http://dx.doi.org/10.1016/j.conbuildmat.2016.02.033
[14] León-Martínez, F.M. – Cano-Barrita, P.F. de J. – Lagunez-Rivera, L. – Medina-Torres, L. (2014) Study of nopal mucilage and marine brown extract as viscosity-enhancing admixtures for cement based materials. Constr Build Mater 53. http://dx.doi.org/10.1016/j.conbuildmat.2013.11.068
[15] Arizzi, A. – Banfill, P.F.G. (2019) Rheology of lime pastes with biopolymer-based additives. Mater Struct 52(8) http://dx.doi.org/10.1617/s11527-019-1310-8
[16] McHugh, D.J: (2003) A guide to the seaweed industry, Food and agriculture organization of the United Nations, Rome
[17] Li, Z., Zhang, L. (2016) Biopolymers and Biotech Admixtures for Eco-Efficient Construction Materials, Woodhead Publishing, Duxford,
[18] Abdollahnejad, Z. – Kheradmand, M. – Pacheco-Torgal, F. (2017) Short-term compressive strength of fly ash and waste glass alkali-activated cement-based binder mortars with two biopolymers. J Mater Civ Eng. 29(7) http:// dx.doi.org/10.1061/(ASCE)MT.1943-5533.0001920
[19] Žižlavský, T. – Vyšvařil, M. – Rovnaníková, P., (2019) Physical-mechanical properties and durability of mortars with non-treditional biopolymers. Acta Polytechnica. 22. http://dx.doi.org/10.14311/APP.2019.22.0150
[20] Cappellari, M. – Daubresse, A. – Chaouche, M. (2013) Influence of organic thickening admixtures on the rheological properties of mortars: Relationship with water-retention. Constr Build Mater 38 http://dx.doi.org/10.1016/j.conbuildmat.2012.09.055
[21] Poinot, T. – Govin, A. – Grosseau, P. (2014) Influence of hydroxypropylguars on rheological behavior of cement-based mortars. Cem Concr Res 58. http://dx.doi.org/10.1016/j.cemconres.2014.01.020
[22] Leeman, A. – Winnefeld, F., (2007) The effect of viscosity modifying agents in mortar and concrete. Cem Concr Compos 29. http://dx.doi.org/10.1016/j.cemconcomp.2007.01.004
[23] Rapp, B.E. (2016) Microfluidics: Modeling, Mechanics and Mathematics. Elsevier Science
[24] Žižlavský, T. – Vyšvařil, M. – Rovnaníková, P. (2019) Rheological study on influence of hydroxypropyl derivatives of guar gum, cellulose, and chitosan on the properties of natural hydraulic lime pastes. IOP Conf Ser Mater Sci Eng 583. http://dx.doi.org/10.1088/1757-899X/583/1/012009
[25] Vyšvařil, M. – Hegrová, M. – Žižlavský, T. (2018) Rheological properties of lime mortars with guar gum derivatives. Key Eng Mater 760. http://dx.doi.org/10.4028/www.scientific.net/KEM.760.257
[26] Vyšvařil, M. – Žižlavský, T. (2017) Effect of chitosan ethers on fresh state properties of lime mortars. IOP Conf Ser Mater Sci Eng 251. http://dx.doi.org/10.1088/1757-899X/251/1/012039

Ref.:
Žižlavský, Tomáš – **Vyšvařil**, Martin – **Rovnaníková**, Pavla: *Rheology of natural hydraulic lime pastes modified by non-traditional biopolymeric admixtures*
Építőanyag – Journal of Silicate Based and Composite Materials, Vol. 71, No. 6 (2019), 204–209. p.
https://doi.org/10.14382/epitoanyag-jsbcm.2019.36

Libál Lajos György
(1938 -2019)

Szomorú szívvel tudatjuk mindazokkal, akik ismerték és szerették, hogy életének 82. évében elhunyt Libál Lajos György, az SZTE Üveg szakosztály régi tagja és támogatója.

Középiskolai tanulmányait Budapesten végezte, majd 1965-ben az ausztriai Leobenben szerzett okl. kohómérnöki diplomát.

1981-től Párizsban a RADEX tűzállóanyag-gyártó cég nemzetközi üzletkötője, majd 1988-tól önálló céget alapított. Ezeken keresztül képviselte az európai üvegipar vezető beszállító cégeit, melyek a Tungsram, majd később a GE Hungary üveggyártása egyik legmegbízhatóbb, magas műszaki színvonalat képviselő partnereivé váltak.

Az évtizedek során a segítségével kiemelkedő tudású, nemzetközileg elismert kutatási, fejlesztési szakemberek tartottak színvonalas előadásokat az SZTE Üveg szakosztály konferenciáin, bemutatva a legújabb - elsősorban német – fejlesztéseket, trendeket az üvegipar területén. Az elmúlt években példamutató, jelentős anyagi felajánlást tett az SZTE rendezvények zökkenőmentes lebonyolításához.

80 éves korán túl is aktív „örökifjú"maradt. 1954 óta vívott, és lett korosztályos országos veteránbajnok párbajtőrvívásban.

Bár hősiesen küzdött ellene, élete utolsó nagy csatájában már nem volt esélye a gyilkos kórral szemben.

Nyugodjék békében!

SZTE Üveg szakosztály

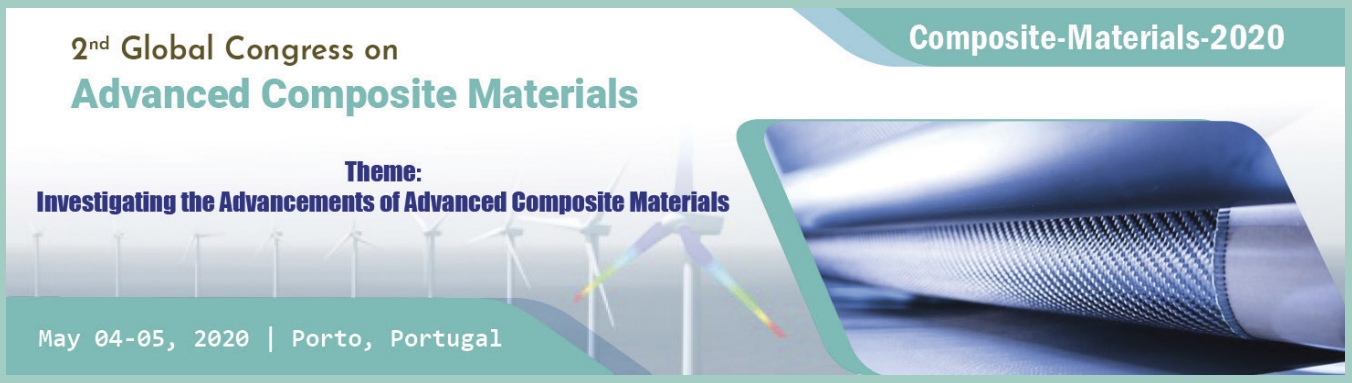

Welcome…!!!

On behalf of the Organizing and Advisory Committee we take great pleasure in welcoming academic scientists, researchers, research scholars, students and experts of application fields to Porto, Portugal for the **2nd Global Congress on Advanced Composite Materials** to foster the progress in the field by contributing with your expertise to what promises to be a very comprehensive and exciting meeting, and to enjoy the immense unique artistic heritage

(Composite Materials-2020), which will be held during May 04-05, 2020 is now an established event, attracting global participant's intent on sharing, exchanging and exploring new avenues of Composite Materials and related research and latest developments. The event will have 5-6 world level (Highly cited class) Plenary speakers, established Keynote speakers, active Invited speakers and fresh contributed speakers. In addition, variety of poster presentations along with workshops and special sessions would be interested in audience.

The aim of the **Composite Materials-2020** is to promote quality research and real-world impact in an atmosphere of true international cooperation between scientists and engineers by bringing together again the world class researchers, International Communities and Industrial heads to discuss the latest developments and innovations in the fields of Composite Materials-2020.

We sincerely hope that **(Composite Materials-2020)** serves as an international platform for meeting researchers from around the world, widen professional contact and create new opportunities, including establishing new collaborations.

Benefits of Composite Materials-2020 conference:

Learn about the latest research in your field

Meet and get to know your peers

Gain visibility in your field

Share your research findings with others in your field

Stay on top of trends and topics

Promote Creativity & Innovation in business field

Global networking In exchanging and trading Ideas

A Unique Opportunity for Advertisers and Sponsors at this International meeting

Grow as a researcher and presenter

Obtain feedback on your research

www.scientificfederation.com/composite-materials-2020/

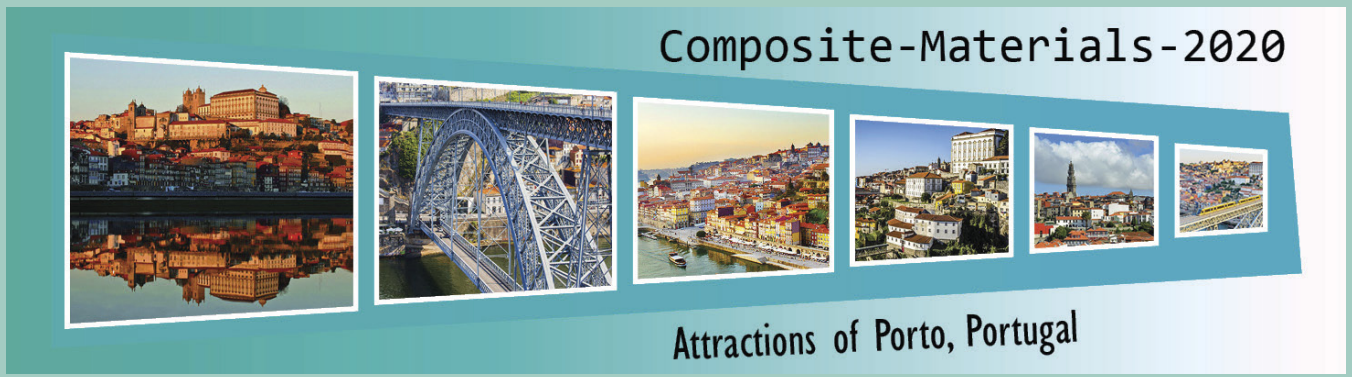

GUIDELINE FOR AUTHORS

The manuscript must contain the followings: title; author's name, workplace, e-mail address; abstract, keywords; main text; acknowledgement (optional)**; references; figures, photos with notes; tables with notes; short biography** (information on the scientific works of the authors).

The full manuscript should not be more than 6 pages including figures, photos and tables. Settings of the word document are: 3 cm margin up and down, 2,5 cm margin left and right. Paper size: A4. Letter size 10 pt, type: Times New Roman. Lines: simple, justified.

TITLE, AUTHOR

The title of the article should be short and objective.

Under the title the name of the author(s), workplace, e-mail address.

If the text originally was a presentation or poster at a conference, it should be marked.

ABSTRACT, KEYWORDS

The abstract is a short summary of the manuscript, about a half page size. The author should give keywords to the text, which are the most important elements of the article.

MAIN TEXT

Contains: materials and experimental procedure (or something similar), results and discussion (or something similar), conclusions.

REFERENCES

References are marked with numbers, e.g. [6], and a bibliography is made by the reference's order. References should be provided together with the DOI if available.

Examples:

Journals:

[6] Mohamed, K. R. – El-Rashidy, Z. M. – Salama, A. A.: In vitro properties of nano-hydroxyapatite/chitosan biocomposites. *Ceramics International.* 37(8), December 2011, pp. 3265–3271, http://doi.org/10.1016/j.ceramint.2011.05.121

Books:

[6] Mehta, P. K. – Monteiro, P. J. M.: Concrete. Microstructure, properties, and materials. *McGraw-Hill*, 2006, 659 p.

FIGURES, TABLES

All drawings, diagrams and photos are figures. The **text should contain references to all figures and tables**. This shows the place of the figure in the text. Please send all the figures in attached files, and not as a part of the text. **All figures and tables should have a title**.

Authors are asked to submit color figures by submission. Black and white figures are suggested to be avoided, however, acceptable.

The figures should be: tiff, jpg or eps files, 300 dpi at least, photos are 600 dpi at least.

BIOGRAPHY

Max. 500 character size professional biography of the author(s).

CHECKING

The editing board checks the articles and informs the authors about suggested modifications. Since the author is responsible for the content of the article, the author is not liable to accept them.

CONTACT

Please send the manuscript in electronic format to the following e-mail address: femgomze@uni-miskolc.hu and epitoanyag@szte.org.hu or by post: Scientific Society of the Silicate Industry, Budapest, Bécsi út 122–124., H-1034, HUNGARY

We kindly ask the authors to give their e-mail address and phone number on behalf of the quick conciliation.

Építőanyag – *Journal of Silicate Based and Composite Materials*, Quarterly peer-reviewed periodical of the Hungarian Scientific Society of the Silicate Industry, SZTE.
http://epitoanyag.org.hu

European Materials Research Society

E-MRS now has more than 4,000 members from industry, government, academia and research laboratories, who meet regularly to debate recent technological developments of functional materials. The E-MRS differs from many single-discipline professional societies by encouraging scientists, engineers and research managers to exchange information on an interdisciplinary platform, and by recognizing professional and technical excellence by promoting awards for achievement from student to senior scientist level. As an adhering body of the International Union of Materials Research Societies (IUMRS), the E-MRS enjoys and benefits from very close relationships with other Materials Research organizations elsewhere in Europe and around the world.

23 RUE DU LOESS, BP 20 - 67037
STRASBOURG CEDEX 02, FRANCE
EMRS@EUROPEAN-MRS.COM
WWW.EUROPEAN-MRS.COM